



THE UNIVERSITY *of* EDINBURGH

Edinburgh Research Explorer

Heparan sulphate sulphation by Hs2st restricts astroglial precursor somal translocation in developing mouse forebrain by a non cell autonomous mechanism

Citation for published version:

Clegg, J, Parkin, H, Mason, J & Pratt, T 2019, 'Heparan sulphate sulphation by Hs2st restricts astroglial precursor somal translocation in developing mouse forebrain by a non cell autonomous mechanism', *Journal of Neuroscience*. <https://doi.org/10.1523/JNEUROSCI.1747-17.2018>

Digital Object Identifier (DOI):

[10.1523/JNEUROSCI.1747-17.2018](https://doi.org/10.1523/JNEUROSCI.1747-17.2018)

Link:

[Link to publication record in Edinburgh Research Explorer](#)

Document Version:

Peer reviewed version

Published In:

Journal of Neuroscience

General rights

Copyright for the publications made accessible via the Edinburgh Research Explorer is retained by the author(s) and / or other copyright owners and it is a condition of accessing these publications that users recognise and abide by the legal requirements associated with these rights.

Take down policy

The University of Edinburgh has made every reasonable effort to ensure that Edinburgh Research Explorer content complies with UK legislation. If you believe that the public display of this file breaches copyright please contact openaccess@ed.ac.uk providing details, and we will remove access to the work immediately and investigate your claim.



Research Articles: Development/Plasticity/Repair

Heparan sulphate sulphation by Hs2st restricts astroglial precursor somal translocation in developing mouse forebrain by a non cell autonomous mechanism

James M. Clegg^{1,2}, Hannah Parkin², John O. Mason^{1,2} and Thomas Pratt^{1,2}

¹*Simons Initiative for the Developing Brain*

²*Centre for Discovery Brain Sciences, Hugh Robson Building, Edinburgh Medical School Biomedical Sciences, The University of Edinburgh, Edinburgh, United Kingdom, EH8 9XD, United Kingdom.*

<https://doi.org/10.1523/JNEUROSCI.1747-17.2018>

Received: 22 June 2017

Revised: 5 December 2018

Accepted: 11 December 2018

Published: 7 January 2019

Author contributions: J.M.C., H.M.P., J.O.M., and T.P. designed research; J.M.C. and H.M.P. performed research; J.M.C. and H.M.P. analyzed data; J.M.C., H.M.P., and T.P. wrote the paper.

Conflict of Interest: The authors declare no competing financial interests.

We are grateful to the following people for supplying us with transgenic mouse lines: **Hs2stfl**, Jeffrey Esko (University College San Diego); **Ext1fl**, Yu Yamaguchi (Sanford Burnham Institute); **Zic4Cre** and **Emx1CreER**, Nicoletta Kessaris (University College London). We would like to thank the anonymous reviewers whose comments have helped us improve the manuscript from its initial submission. This work was supported by grants from The Wellcome Trust (094832/Z/10/Z) and BBSRC (BB/M00693X/1) to TP and an EASTBIO BBSRC funded PhD studentship to HP.

Correspondence should be addressed to Senior Author and correspondence: t.pratt@ed.ac.uk

Cite as: J. Neurosci 2019; 10.1523/JNEUROSCI.1747-17.2018

Alerts: Sign up at www.jneurosci.org/alerts to receive customized email alerts when the fully formatted version of this article is published.

Accepted manuscripts are peer-reviewed but have not been through the copyediting, formatting, or proofreading process.

Copyright © 2019 Clegg et al.

This is an open-access article distributed under the terms of the Creative Commons Attribution 4.0 International license, which permits unrestricted use, distribution and reproduction in any medium provided that the original work is properly attributed.

1 **Title Page.**

2 **Title:** Heparan sulphate sulphation by Hs2st restricts astroglial precursor somal
 3 translocation in developing mouse forebrain by a non cell autonomous mechanism.

4 **Abbreviated title:** Hs2st and FGF signalling in developing mouse brain.

5 **James M. Clegg**^{1,2,3}, **Hannah Parkin**^{2,3}, **John O. Mason**^{1,2}, and **Thomas Pratt**^{1,2,4}

6 ¹Simons Initiative for the Developing Brain,

7 ²Centre for Discovery Brain Sciences,

8 Hugh Robson Building, Edinburgh Medical School Biomedical Sciences, The University
 9 of Edinburgh, Edinburgh, United Kingdom, EH8 9XD, United Kingdom.

10 ³These authors contributed equally to this work

11 ⁴Senior Author and correspondence: t.pratt@ed.ac.uk

12 **Number of Pages (excluding figures):** 34

13 **Number of figures:** 11

14
 15 **Number of words:**

16 **Abstract:** 250

17 **Introduction:** 780

18 **Discussion:** 2122

19
 20 **Conflict of interest:** The authors declare no competing financial interests

21
 22 **Acknowledgements:** We are grateful to the following people for supplying us with
 23 transgenic mouse lines: *Hs2st*^{fl}, Jeffrey Esko (University College San Diego); *Ext1*^{fl}, Yu
 24 Yamaguchi (Sanford Burnham Institute); *Zic4*^{Cre} and *Emx1*^{CreER}, Nicoletta Kessaris
 25 (University College London). We would like to thank the anonymous reviewers whose
 26 comments have helped us improve the manuscript from its initial submission. This work was
 27 supported by grants from The Wellcome Trust (094832/Z/10/Z) and BBSRC
 28 (BB/M00693X/1) to TP and an EASTBIO BBSRC funded PhD studentship to HP.

29
 30 **Abstract**

31 Heparan sulphate (HS) is a cell surface and extracellular matrix carbohydrate extensively
 32 modified by differential sulphation. HS interacts physically with canonical fibroblast growth
 33 factor (FGF) proteins that signal through the extracellular signal regulated kinase

(ERK)/mitogen activated kinase (MAPK) pathway. At the embryonic mouse telencephalic midline FGF/ERK signalling drives astroglial precursor somal translocation from the ventricular zone of the cortico-septal boundary (CSB) to the induseum griseum (IG) producing a focus of *Slit2*-expressing astroglial guidepost cells essential for inter-hemispheric corpus callosum (CC) axon navigation. Here we investigate the cell and molecular function of a specific form of HS sulphation, 2-O HS sulphation catalysed by the enzyme Hs2st, in midline astroglial development and in regulating FGF protein levels and interaction with HS. *Hs2st*^{-/-} embryos of either sex exhibit a grossly enlarged IG due to precocious astroglial translocation and conditional *Hs2st* mutagenesis and *ex vivo* culture experiments show that *Hs2st* is not required cell autonomously by CC axons or by the IG astroglial cell lineage but rather acts non cell autonomously to suppress the transmission of translocation signals to astroglial precursors. Rescue of the *Hs2st*^{-/-} astroglial translocation phenotype by pharmacologically inhibiting FGF signalling shows the normal role of Hs2st is to suppress FGF-mediated astroglial translocation. We demonstrate a selective action of Hs2st on FGF protein by showing that *Hs2st* (but not *Hs6st1*) normally suppresses the levels of Fgf17 protein in the CSB region *in vivo* and use a biochemical assay to show *Hs2st* (but not *Hs6st1*) facilitates physical interaction between Fgf17 protein and HS.

Significance statement.

We report a novel non cell autonomous mechanism regulating cell signalling in developing brain. Using the developing mouse telencephalic midline as an exemplar we show that the specific sulphation modification of the cell surface and extracellular carbohydrate heparan sulphate (HS) performed by Hs2st suppresses the supply of translocation signals to astroglial precursors by a non cell autonomous mechanism. We further show that Hs2st modification selectively facilitates physical interaction between Fgf17 and HS and suppresses Fgf17 protein levels *in vivo*, strongly suggesting that Hs2st acts selectively on Fgf17 signalling. HS interacts with many signalling proteins potentially encoding numerous selective interactions important in development and disease so this class of mechanism may apply more broadly to other biological systems.

Introduction

The corpus callosum (CC) axon tract connects the cerebral hemispheres through the cortico-septal boundary (CSB) in mice and humans and CC malformation is associated with cognitive and neurological conditions in humans (Donahoo and Richards, 2009). Precisely

controlled radial glial cell (RGC) somal translocation from the ventricular zone (VZ) of the CSB to its pial surface generates midline zipper (MZ) and induium griseum (IG) astroglial populations required for cerebral hemisphere fusion and subsequent CC axon navigation (Clegg et al., 2014; Gobius et al., 2016; Inatani et al., 2003; Moldrich et al., 2010; Shu and Richards, 2001; Shu et al., 2003; Smith et al., 2006). The movement of RGC astroglial precursors from the glial wedge (GW) to the IG (GW→IG translocation) forms an astroglial guidepost population that secretes Slit2 to guide CC axons across the telencephalic midline.

Fibroblast growth factors (FGFs) are an evolutionarily ancient family comprising 23 genes in mice and humans of which 15 (*Fgfl-10,16-18,20,22* in mice) encode ‘canonical’ FGFs that function as paracrine signalling molecules and bind promiscuously to cell surface FGF receptors (FGFRs encoded by *Fgfr1-4* in mice) to elicit an extracellular signal regulated kinase (ERK)/mitogen activated kinase (MAPK) response via activating phosphorylation of ERK→phospho-ERK (pERK). Canonical FGFs are further subdivided into five subfamilies based on phylogeny and ‘*Fgf8*’ subfamily members *Fgf8* and *Fgf17* are transcribed in the developing CSB in close spatiotemporal proximity posing the question of how they are coordinated (Guillemot and Zimmer, 2011; Ornitz and Itoh, 2015). Under normal conditions GW→IG translocation is primarily attributed to *Fgf8* and needs to be tightly regulated to ensure correct numbers of RGCs leave the GW and reach the IG. Deviation above (or below) normal FGF/ERK signalling levels induces too many (or too few) RGCs to translocate with consequent disruption to CC development (Clegg et al., 2014; Gobius et al., 2016; Smith et al., 2006; Wang et al., 2012). While *Fgf17* plays a role in patterning the developing telencephalon its importance for CC development is less clear and no CC phenotype has been reported in *Fgf17*^{-/-} embryos (Cholfin and Rubenstein, 2007, 2008). Because *Fgf8* and *Fgf17* are the principal *Fgf*’s transcribed in vicinity of the GW and both activate ERK, mechanisms must exist to keep the total amount of Fgf protein (*Fgf8* protein + *Fgf17* protein) at the correct level to generate the correct levels of ERK activation for astroglial precursor RGCs to translocate in appropriate numbers.

Heparan sulphate (HS), the carbohydrate component of cell surface and extracellular matrix (ECM) heparan sulphate proteoglycans, is a negatively charged sulphated polysaccharide that binds canonical FGFs in the ECM to regulate their movement and half-life and also functions as an obligate FGF co-receptor in FGF:FGFR:HS ternary signalling complexes on the cell surface (Balasubramanian and Zhang, 2016; Guillemot and Zimmer, 2011). HS biosynthesis is in two stages, Ext enzymes polymerise uronic acid – glucosamine disaccharides making linear [uronic acid – glucosamine]_n HS polymers which are then

modified by the enzymatic addition (by heparan sulphate sulphotransferases, HSTs) or removal (by heparan sulphate sulphatases, Sulfs) of sulphate groups at specific positions on the disaccharide residues. There are four classes of HST enzymes (Hs2st, Hs3st, Hs6st, and Ndst) each adding sulphate to a specific position, for example Hs2st only adds sulphate to the carbon atom in position 2 of uronic acid generating 2-O HS sulphation. While work in a variety of systems shows that HS itself can play roles both in the transmission of FGF signals through the ECM (non cell autonomous role) and the cellular response to FGF (cell autonomous role) the potential for specific forms of HS sulphation to selectively regulate FGFs by regulating the physical interaction between HS and FGF proteins is much less well understood (Allen et al., 2001; Allen and Rapraeger, 2003; Balasubramanian and Zhang, 2016; Belenkaya et al., 2004; Chan et al., 2015; Chan et al., 2017; Christian, 2012; Guillemot and Zimmer, 2011; Kinnunen et al., 2005; Loo et al., 2001; Loo and Salmivirta, 2002; Makarenkova et al., 2009; Qu et al., 2011; Qu et al., 2012; Ramsbottom et al., 2014; Toyoda et al., 2011; Yan and Lin, 2009; Yu et al., 2009; Zhang et al., 2012a).

The heparan sulphate code hypothesis states that different forms of HS sulphation can encode specific instructions (Kreuger et al., 2006; Turnbull et al., 2001). In this study we discover that 2-O HS sulphation catalysed by Hs2st functions non cell autonomously at the developing telencephalic midline to suppress FGF/ERK signalling that drives the somal translocation of astroglial precursors required for normal CC development and present evidence that Hs2st plays a selective role by modulating the physical interaction between Fgf17 protein and HS and selectively suppressing Fgf17 protein levels at the CSB.

Materials and Methods

Animals: All mice were bred in-house in line with Home Office UK legislation and licences approved by the University of Edinburgh Ethical Review Committees and Home Office. Embryos analysed in this study were of either sex. Animal husbandry was in accordance with UK Animals (Scientific Procedures) Act 1986 regulations. The *Hs2st* LacZ (*Hs2st*⁻) null allele comprised a *LacZ* gene trap vector integrated into the *Hs2st* locus, the *Hs6st1* LacZiresPLAP (*Hs6st1*⁻) null allele comprised a *LacZiresPLAP* gene trap vector integrated in the *Hs6st1* locus, both were genotyped by PCR as previously described (Bullock et al., 1998; Conway et al., 2011; Pratt et al., 2006). For some *ex vivo* experiments *Hs2st*^{+/-} mice were crossed with mice carrying the TP6.3 Tau (τ) -GFP fusion transgene to generate *Hs2st*^{-/-} and *Hs2st*^{+/-} embryos with τGFP⁺ axons (Pratt et al., 2000). For conditional mutagenesis floxed

135 *Ext1* (*Ext1^{fl}*) or *Hs2st* (*Hs2st^{fl}*) alleles were combined with either *Zic4^{Cre}* (septal deletion) or
 136 *Emx1^{CreER}* (cortical deletion) driver alleles (Inatani et al., 2003; Kessaris et al., 2006; Rubin et
 137 al., 2010; Stanford et al.). *CreER* activity was induced at E9.5 by administering tamoxifen
 138 (dissolved in corn oil using a sonicator) to pregnant dams by intraperitoneal (IP) injection
 139 (120mg/kg dose). Lineages of cells in which Cre was active were visualised using a
 140 Rosa26R-floxed-stop-EGFP reporter allele (Sousa et al., 2009).

141 **Ex vivo assays:** *Ex vivo* culture experiments were performed essentially as described
 142 previously (Niquille et al., 2009). Explants were cultured on nucleopore polycarbonate
 143 membranes (Whatman) floating on 1 ml ‘Neurobasal media’ (Neurobasal medium (Life
 144 Technologies) supplemented with L-glutamine, glucose and penicillin/streptomycin) at 37°C
 145 with 5% CO₂ in a humidified incubator. Brains were dissected from embryos in oxygenated
 146 Earle’s balanced salt solution (Life Technologies), embedded in low melting point agarose,
 147 sliced using a vibratome (Leica VTS-1000), and transferred to Modified Eagle medium
 148 (MEM, Life Technologies) with 5% foetal bovine serum for 1 hour. For CC axon navigation
 149 assays 400µm thick E17.5 coronal slices incorporating the CC axon tract were prepared and
 150 frontal cortex explants from τ -GFP⁺ slices were transplanted into the equivalent region in τ -
 151 GFP⁻ slices prior to culturing in Neurobasal media for 72 hours, fixation in 4%
 152 paraformaldehyde (PFA), and GFP immunofluorescence. For glial translocation experiments
 153 10 mg/ml BrdU dissolved in PBS was injected IP into pregnant dams with E14.5 litters which
 154 were sacrificed 1 hour later and 350µm coronal slices incorporating the CSB prepared for
 155 culture. In Fgf17 bead experiments Affi-gel blue gel (Bio-rad) beads pre-soaked in 100µg/ml
 156 recombinant Fgf17 protein (R&D systems) or 5mg/ml BSA (Sigma) overnight at 4°C were
 157 implanted into the slice, one Fgf17 and one BSA bead on either side of the midline just below
 158 the GW, and the MEM replaced with Neurobasal media. For the FGF_i culture, MEM media
 159 was replaced with Neurobasal media containing either 25µM SU5402, 0.1% DMSO (FGF
 160 inhibitor (FGF_i) treated) or 0.1% DMSO (control). Slices were cultured for 2 or 48 hours,
 161 fixed in 4% PFA, and 10µm frozen sections prepared for immuno-detection or *in situ*
 162 hybridisation. Glial migration out of the VZ towards the pial surface was quantified from
 163 BrdU/Sox9 immunofluorescence micrographs by demarcating the basal edge of the VZ
 164 (easily identified by Sox9 staining) with a line and counting the number of Sox9⁺;BrdU⁺ cells
 165 which had crossed this line. This allowed us to count glial (Sox9⁺) cells that had incorporated
 166 BrdU (BrdU⁺) when they were in the VZ before the start of the culture and subsequently
 167 exited the VZ and migrated towards the midline over the 2 day culture period when the

168 cultures were exposed to experimental substances (SU5402, DMSO, Fgf17 protein, or BSA).
 169 4 or 6 sections were quantified per slice moving rostrally from the most caudal section in
 170 which the GW could be identified on both sides of the section.

171 **Immunodetection:** Embryonic mouse brains were removed and fixed in 4% PFA in PBS
 172 overnight at 4°C, cryoprotected in 30% sucrose in PBS, embedded in OCT, and 10µm
 173 coronal frozen sections cut using a cryostat (Leica). Immunohistochemistry was performed as
 174 described previously (Clegg et al., 2014). Primary antibodies: goat anti-GFP (diluted 1/250,
 175 Abcam); rabbit anti-Sox9 (1/500, Cell Signalling Technologies); rat anti-L1 (1/200,
 176 Millipore); rabbit anti-GFAP (1/200 Dako); rabbit anti-Hs2st (1/50, Abcam ab103120); rabbit
 177 anti-Fgf17 (1/1000, Abcam ab187982); and rabbit anti-pErk1/2 (1/200, Cell signalling).
 178 Secondary antibodies; donkey anti-goat Alexa Fluor 488; donkey anti-rabbit Alexa Fluor
 179 568; and goat anti-rat 568 (all used at a dilution of 1/200 and from Invitrogen). Fluorescently
 180 labelled sections were counterstained with DAPI (Invitrogen). For Hs2st and pErk1/2
 181 antibody staining goat anti-rabbit biotin secondary antibody (1/200, Vector Laboratories) was
 182 used and staining was visualised using a standard avidin-biotin diaminobenzidine (DAB)
 183 staining procedure. The Fgf17 immunofluorescence was performed using exactly the same
 184 protocol as previously described for Fgf8 except that the Fgf8 antibody was replaced with the
 185 Fgf17 antibody (Clegg et al., 2014; Toyoda et al., 2011). Briefly, slides were first washed in
 186 acetone for permeabilisation, Rabbit Fgf17 antibody applied, and the TSA plus Fluorescence
 187 System kit (Perkin Elmer) used for fluorescence detection.

188 **In situ Hybridisation:** *In situ* hybridisation was carried out on 10µm frozen sections as
 189 previously described (Wallace and Raff, 1999) using digoxigenin-labelled riboprobes for
 190 *Slit2* and *Fgf17* (Erskine et al., 2000; Xu et al., 1999).

191 **Imaging:** Fluorescent labelled sections were imaged using either a Leica AF6000
 192 epifluorescence microscope coupled to a Leica DFC360 digital camera or a Nikon Ti: E
 193 Inverted confocal microscope. DAB stained and in situ hybridised sections were imaged
 194 using a Leica DLMB microscope coupled to a Leica DFC480 colour digital camera.

195 **Fgf17 protein quantification:** Fgf17 fluorescence was quantified from E14.5
 196 *Hs2st*^{+/+}; *Hs6st1*^{+/+}, *Hs2st*^{-/-} and *Hs6st1*^{-/-} coronal sections that had been processed for Fgf17
 197 immunofluorescence in parallel and imaged under identical conditions in parallel using the
 198 same method as previously described for Fgf8 protein quantification (Chan et al., 2017). For
 199 each section IMAGE J was used to measure mean fluorescence intensity in a 100 x 150 µm

200 box drawn at the CSB encompassing the Fgf17 expression domain. For each embryo
201 quantification was performed for three sections along the rostro-caudal axis and averaged.

202 **IG Sox9⁺ cell quantification:** Quantification of Sox9 immunofluorescent positive cells
203 (Sox9⁺ cells) in the IG region of E18.5 *Hs2st^{fl/fl};Zic4^{Cre}*, *Hs2st^{+/+};Zic4^{Cre}* *Hs2st^{fl/fl};Emx1^{CreER}*,
204 and *Hs2st^{+/+};Emx1^{CreER}* embryos were performed as previously described (Clegg et al.,
205 2014). A counting box measuring 200µm x 200µm was placed on images of coronal sections
206 at the midline with the top edge at the dorsal extent of Sox9⁺ cells at the IG and the numbers
207 of Sox9⁺ cells in the box counted. For each embryo quantification was performed for three
208 sections along the rostro-caudal axis and averaged.

209 **Western Blotting:** Western blotting was performed as previously described (Clegg et al.,
210 2014), primary antibodies: rabbit anti-Hs2st (1/500, Abcam ab103120) and mouse anti-β-
211 actin (1/5000, Abcam). Secondary antibodies: goat anti-mouse Alexa Fluor 680 (Invitrogen)
212 and goat anti-rabbit 800 (Li-Cor).

213 **Ligand and Carbohydrate Engagement (LACE) Assay:** LACE assay was performed as
214 previously described (Allen et al., 2001; Allen and Rapraeger, 2003; Chan et al., 2015).
215 Briefly, frozen sections were incubated in 0.05% NABH₄/PBS for 15 min. After several
216 washes in PBS, sections were incubated in 0.1M glycine at 4°C overnight. Some sections
217 were incubated with Heparitinase I (Seikagaku) before proceeding. All Fgf and Fgfr-Fc
218 proteins were purchased from R&D Systems. Sections were then treated with 1% BSA/TBS
219 solution for 10 min before incubation with 3 µM recombinant mouse Fgf17 and 9 µM
220 recombinant human Fgfr1a(IIIc)-Fc or 30nM recombinant mouse Fgf8b and 100nM
221 recombinant human Fgfr3 (IIIc)-Fc at 4°C overnight. Fgf17 or Fgf8 were omitted from some
222 assays. Fluorescent LACE signal was generated by incubation with 1/200 anti-human IgG
223 (Fc-specific) Cy3 (Sigma) in 1% BSA/TBS. *Hs2st^{+/+};Hs6st1^{+/+}*, *Hs2st^{-/-}* and *Hs6st1^{-/-}*
224 material that had been processed for each LACE assay condition in parallel were imaged
225 under identical conditions in parallel. For each section IMAGE J was used to measure mean
226 fluorescence intensity in a 100 x 150 µm box drawn encompassing the CSB. Background
227 signal was quantified from control LACE experiments from which the FGF ligand was
228 omitted and these values used for background subtraction. For each embryo quantification
229 was performed for three sections along the rostro-caudal axis and averaged.

230 **Data analysis and statistics:** Results are expressed as mean ±SEM. The statistical test and
231 sample size (n) for each experiment are specified in the figure legends. Statistical comparison

between 2 groups was performed with a t-test. Statistical comparison between > 2 groups was performed with ANOVA followed by post-hoc t-test. $p < 0.05$ was considered significant.

Results

Hs2st protein is widely expressed in the developing cerebral cortex and at the telencephalic midline.

In order to establish potential sites of action of Hs2st in CC development we first examined the distribution of cells expressing Hs2st protein and contributing to developing CC structures using Hs2st immunohistochemistry at E14.5 (Fig 1 A-D) and E18.5 (Fig 1 E-M) spanning the period of CC axon tract development. Macroscopically, Hs2st protein distribution closely resembles the *Hs2st-LacZ* reporter staining previously reported with widespread Hs2st expression in the developing cerebral cortex and at the CSB at both E14.5 and E18.5 (Fig 1A,E, boxed areas indicate regions shown at higher magnifications in B-D and F-M) (Conway et al., 2011). Subcellularly the Hs2st signal is punctate consistent with the expected localisation of Hs2st in the Golgi apparatus (arrows point to Hs2st⁺ puncta in higher magnification insets in Fig 1B,F,P). At E14.5 there was a high density of Hs2st⁺ puncta at the CSB in the GW region where IG astroglial RGC precursors reside (Fig 1B with boxed area shown as higher magnification inset with arrows indicating Hs2st⁺ puncta) with the density falling towards the pial surface although Hs2st⁺ puncta were visible. There were many Hs2st⁺ puncta in the VZ of the cerebral cortex (Fig 1C) and also in the cortical plate (Fig 1D) indicating that many cortical progenitors and post-mitotic neurones express Hs2st. At E18.5 Hs2st is expressed by many cells in the IG (Fig 1F) and at the apical surface of the ventricular zone (VZ) at the GW (Fig 1G), septum (Fig 1H), and ventral telencephalon (Fig 1I) with the number of Hs2st expressing VZ cells diminishing as distance from the ventricle increases. In the cerebral cortex Hs2st is expressed by many cells close to the apical surface of the VZ (Fig 1J). Large numbers of post-mitotic cortical neurons outside the VZ express Hs2st and moving towards the pial surface the density of Hs2st⁺ puncta varies with laminar position (compare Fig 1 K,L,M showing relatively high Hs2st⁺ puncta density in cortical layers adjacent to the pial membrane (M) and in the intermediate zone (K) and lower density in the intervening region (L)). We validated the Hs2st antibody by demonstrating absence of the punctate Hs2st⁺ immunostaining in *Hs2st*^{-/-} embryonic material (compare Fig 1N,P to O,Q – note that the more diffuse staining persists in *Hs2st*^{-/-} tissue and we discounted this as non-specific background) and western blot showing that the predicted 42kDa Hs2st protein band was present in *Hs2st*^{+/+} and absent from *Hs2st*^{-/-} telencephalic protein extracts (Fig 1R). To

conclude, Hs2st protein is present in developing cerebral cortex, the source of CC axons, as well as in progenitor and post-mitotic cells of the CSB region constituting the environment through which midline crossing CC axons navigate. The Hs2st expression analysis suggests multiple potential sites of action for 2-O HS sulphation in CC development.

The *Slit2* expressing IG is expanded in *Hs2st*^{-/-} embryos.

We previously reported that increased numbers of astroglia at the pial surface of the *Hs2st*^{-/-} CSB stemmed from precocious glial translocation and found no evidence that changes in cell proliferation or death contributed to this phenotype (Clegg et al., 2014; Conway et al., 2011). In order to determine whether there is an expansion of the IG in *Hs2st*^{-/-} embryos we compared the expression of *Slit2* mRNA, a marker of GW and IG glia but not MZ glia, between *Hs2st*^{+/+} and *Hs2st*^{-/-} embryos at E16.5 (Shu and Richards, 2001; Shu et al., 2003). In *Hs2st*^{+/+} embryos *Slit2*⁺ cells form a compact focus at the IG that increases in size moving caudally (Fig 2 A,C,E – *Slit2* expression domain at IG indicated by brackets). In *Hs2st*^{-/-} embryos the *Slit2* expression domain is greatly expanded at the pial surface along the rostro-caudal axis (Fig 2 B,D,F – expanded *Slit2* expression domain indicated by brackets). We conclude that an expansion of the *Slit2*⁺ IG astroglial population makes a major contribution to the *Hs2st*^{-/-} phenotype.

Cell autonomy of HS and 2-O HS sulphation in astroglial precursor somal translocation and corpus callosum development.

We next exploited conditional mutagenesis of *Hs2st* or *Ext1* to experimentally uncouple specific functions of 2-O sulphation from more general functions of HS in astroglial precursor translocation and corpus callosum development. Widespread expression of HS and 2-O HS sulphation leaves open the possibility that each regulates GW→IG astroglial precursor somal translocation cell autonomously by modulating the response to signals, non cell autonomously by regulating the supply of signals, or both. To resolve this we identified two *Cre* alleles, *Zic4*^{Cre} and *Emx1*^{CreER}, that drive *LoxP* mediated mutagenesis in the astroglial lineage or in their cellular environment respectively and used them to conditionally ablate either HS (*Ext1*^{LoxP} mutagenesis) or 2-O HS sulphation (*Hs2st*^{LoxP} mutagenesis) to test for cell autonomous or non cell autonomous functions. We refer to these as ‘*Zic4* lineage’ and ‘*Emx1* lineage’ and next present their characterisation using a floxed-stop GFP reporter that turns on GFP expression in *Cre* expressing cells and their descendants before describing experiments where they are employed to conditionally generate loss of function mutations in

299 *Ext1^{Fl}* or *Hs2st^{Fl}* alleles (Inatani et al., 2003; Kessaris et al., 2006; Rubin et al., 2010; Sousa
300 et al., 2009; Stanford et al.).

301

302 **Characterisation of *Zic4* and *Emx1* lineages.**

303 The septum is of *Zic4* lineage, as shown by strong expression of the GFP reporter (Fig
304 3A). The GFP signal in the intermediate zone of the cerebral cortex (asterisks, Fig. 3A) is due
305 to GFP⁺ thalamocortical axons that project from *Zic4* lineage cells in the thalamus and cells
306 of sub-cortical origin as previously reported (Rubin et al., 2010). At the midline GFP⁺ cells of
307 the *Zic4* lineage are predominantly located ventral to the CSB (dashed lines in Fig 3B) but
308 there is also GFP expression in the IG (boxed area 'D' in Fig 3B). Sox9 is a transcription
309 factor that marks the nuclei of RGCs in the VZ and differentiated astroglia in the IG and
310 MZG and we previously showed that the positioning of Sox9⁺ cells is of critical importance
311 for the development of the CC (Clegg et al., 2014). Combining GFP with Sox9
312 immunostaining reveals the contribution of the *Zic4* lineage to the CSB astroglial
313 populations. There is a sharp boundary (dashed line in Fig 3C) in the VZ of the CSB between
314 Sox9⁺;GFP⁺ cells (arrowheads in Fig 3C) on the septal side and Sox9⁺;GFP⁻ cells (arrows in
315 Fig 3C) on the cortical side. Virtually all the Sox9⁺ cells in the IG (Fig 3D) and MZG (fig 3E)
316 are also GFP⁺ (arrowheads in Fig 3D,E) indicating that these cells are *Zic4* lineage. These
317 data show that the *Zic4* lineage contributes Sox9⁺ cells to the septal VZ and strikingly is the
318 sole source of Sox9⁺ astroglia in the IG (Fig 3F).

319 To mark the *Emx1* lineage, tamoxifen was administered to *Emx1^{CreER}* embryos
320 harbouring the floxed-stop GFP reporter at E9.5 so that early *Emx1* expressing cerebral
321 cortex progenitors and their descendants were rendered GFP⁺. Examination of the expression
322 of the GFP reporter shows that, as expected, the developing cerebral cortex and CC axons are
323 of *Emx1* lineage (Fig. 3G) and that at the midline GFP expression is predominantly located
324 dorsal to the CSB (dashed lines in Fig 3H). Higher magnification shows that there is a sharp
325 boundary between GFP⁺ and GFP⁻ cells at the VZ of the CSB (dashed line in Fig 3I).
326 Combining Sox9 and GFP immunostaining reveals the contribution of the *Emx1* lineage to
327 Sox9⁺ cells. Sox9⁺;GFP⁺ cells (arrowheads in Fig 3I) populate the VZ on the cortical side of
328 the boundary with Sox9⁺;GFP⁻ cells on the septal side (arrows in Fig 3I) showing that the
329 *Emx1* lineage contributes Sox9⁺ cells exclusively to the cortical side of the VZ. All Sox9⁺
330 cells in the IG (Fig 3J) and MZ (Fig 3K) are GFP⁻ (arrows in Fig 3J,K) indicating that the
331 *Emx1* lineage does not contribute Sox9⁺ cells to the IG. These data show that the *Emx1*

lineage contributes Sox9⁺ cells to the cortical VZ but no cells of this lineage contribute Sox9⁺ astroglia to the IG (schema in Fig 3L).

***Ext1* is required by both *Emx1* and *Zic4* lineage cells for corpus callosum development.**

To determine the cellular requirement for HS we deleted *Ext1*, essential for HS synthesis, in the *Zic4* or *Emx1* lineages. In control embryos L1 immunostaining labels axons in the U-shaped CC while GFAP staining labels midline astroglial structures (Fig. 4A with higher magnification of IG and GW in Fig 4D,G). Removing HS from either the *Zic4* lineage (Fig 4B with higher magnification of IG and GW in Fig 4E,H) or the *Emx1* lineage (Fig 4C with higher magnification of IG and GW in Fig 4F,I) generates a severe CC agenesis phenotype (*Zic4*^{Cre};*Ext1*^{FL/FL} n=4/4; *Emx1*^{CreER};*Ext1*^{FL/FL} n=3/3). In *Emx1* conditional mutants (*Emx1*^{CreER};*Ext1*^{FL/FL}) CC axons fail to cross the midline and form Probst bundles (P) some distance short of the midline (Fig. 4B). GFAP⁺ astroglial cells are present in the IG (Fig 4E) and at the GW (fig 4H) in a pattern grossly similar to that of controls (compare Fig. 4D,G to E,H). In *Zic4* conditional mutants (*Zic4*^{Cre};*Ext1*^{FL/FL}) CC axons approach the midline but fail to cross (Fig. 4C with higher magnification of IG and GW in Fig 4F,I). Astroglial populations in *Zic4* conditional mutants are obviously disrupted with less intense GFAP staining at the midline (compare IG region in Fig 4 D to F) and more GFAP at the GW than in controls (arrows in Fig 4I, compare Fig. 4G to I) suggesting that in these embryos astroglial precursors translocate less efficiently to the IG and instead remain in the GW. We noted that the cerebral cortex of *Zic4*^{Cre};*Ext1*^{FL/FL} brains was thinned and the ventricles were enlarged (compare Fig4 A to C), this hydrocephalus-like phenotype is intriguing because the cerebral cortex is not of the *Zic4* lineage indicating a non-cell autonomous mechanism by which HS regulates cerebral cortex development. The FGFR1/ FGF2 ligand and carbohydrate engagement (LACE) assay detects endogenous HS on tissue sections by forming ternary complexes with exogenously added FGF2 and FGFR1 (red LACE signal in Fig 4 J-O) (Allen et al., 2001; Chan et al., 2015). HS is ubiquitously expressed in both cortical and septal compartments of control telencephalon (Fig 4J, higher magnification of CSB in M) and, as intended, HS synthesis is blocked in the cortex and cortical axons of *Emx1*^{CreER};*Ext1*^{FL/FL} embryos (Fig 4K, CSB shown at higher magnification in N with arrows indicating HS deficient cortical region) and in the septum of *Zic4*^{Cre};*Ext1*^{FL/FL} embryos (Fig 4L, higher magnification of CSB in O with arrows indicating HS deficient septum). Predigesting tissue sections with heparitinase eliminated the LACE signal (not shown) confirming specificity of this assay for detecting HS. The salient conclusions from the *Ext1* conditional mutagenesis

for the current study are that HS is indispensable from both the *Zic4* and the *Emx1* lineages for CC development and that removing HS from the *Zic4* lineage inhibits *Zic4* lineage astroglia reaching the IG region.

***Hs2st* is required by *Emx1* lineage but not *Zic4* lineage cells for corpus callosum development.**

Having established that both *Zic4* and *Emx1* lineages need to synthesise HS for normal CC development we next asked whether 2-O HS sulphation of the HS is required in either lineage. *Hs2st* is the sole enzyme capable of imparting 2-O HS sulphation onto HS so to determine the cellular requirement for 2-O HS sulphation we deleted *Hs2st* in the *Zic4* or *Emx1* lineages. Control *Hs2st*^{+/+} genotypes (*Hs2st*^{+/+};*Emx1*^{CreER} and *Hs2st*^{+/+};*Zic4*^{Cre}) displayed neither CC agenesis nor midline astroglial disorganisation, the control embryo shown in Fig 5 (A,D,G,J – D,G reproduced from Fig 3 H,J) is *Hs2st*^{+/+};*Emx1*^{CreER} genotype. The CC and the midline astroglial structures form normally in *Hs2st*^{fl/fl};*Zic4*^{Cre} conditional mutants and the organisation of L1⁺ axons and GFAP⁺ astroglia are indistinguishable from control embryos (6/6 embryos) (Fig. 5B, compare to control in 5A). The organisation of GFP⁺ *Zic4* lineage cells is the same in *Hs2st*^{fl/fl};*Zic4*^{Cre} embryos as in *Hs2st*^{+/+};*Zic4*^{Cre} embryos (compare Fig 5E,H to Fig 3B,D) and IG Sox9⁺ cell counts confirm that the numbers of Sox9⁺ cells in the IG are not significantly different to control *Hs2st*^{+/+} embryos (Fig 5M, compare blue and orange bars) indicating no cell autonomous requirement for *Hs2st* in the *Zic4* lineage Sox9⁺ IG astroglia. To exclude the possibility of a compensatory mechanism by which the *Hs2st*^{fl/fl};*Zic4*^{Cre} IG is populated by *Hs2st*^{+/+} cells from a different lineage we performed *Hs2st* immunohistochemistry and confirmed that *Hs2st* expression is indeed absent from all cells in the IG (Fig 5K, note this is an adjacent section from the same embryo to the one shown in 5H). In *Hs2st*^{fl/fl};*Emx1*^{CreER} embryos the CC fails to form in approximately 50% of cases, embryos either had a severe phenotype (Fig 5C, 5/9 embryos) or appeared completely unaffected (Fig 5C', 4/9 embryos). CC axons form Probst bundles (P) on either side of the telencephalic midline while the GFAP⁺ IG is expanded (asterisks, Fig. 5C). The anatomy and incomplete penetrance of the CC phenotype in *Hs2st*^{fl/fl};*Emx1*^{CreER} embryos closely resemble constitutive null *Hs2st*^{-/-} embryos indicating that *Hs2st* function within the *Emx1* lineage is sufficient for normal CC development (Clegg et al., 2014; Conway et al., 2011). As in control *Hs2st*^{+/+};*Emx1*^{CreER} embryos (Fig 5 D,G) the GFP and Sox9 signals did not overlap in the IG region of control or *Hs2st*^{fl/fl};*Emx1*^{CreER} embryos (Fig 5F, boxed area shown at higher magnification in 5I) and the Sox9⁺ cells in the IG of control

embryos and the expanded IG of *Hs2st*^{fl/fl};*Emx1*^{CreER} embryos were GFP⁺ (arrows in Fig 5I indicate Sox9⁺;GFP⁺ cells). Counts of Sox9⁺ cells confirmed a significant increase in the IG of affected *Hs2st*^{fl/fl};*Emx1*^{CreER} embryos compared to controls (Fig 5M, compare blue and purple bars). Immunostaining for Hs2st on adjacent sections confirmed that IG cells in *Hs2st*^{fl/fl};*Emx1*^{CreER} embryos retain Hs2st protein expression (Fig 5L). Because Sox9⁺ IG astroglia do not belong to the *Emx1* lineage their ectopic position in *Hs2st*^{fl/fl};*Emx1*^{CreER} embryos, despite retaining *Hs2st* function, allows us to conclude a cell non autonomous requirement for Hs2st in the translocation of astroglial precursors to the IG..

The salient conclusions from these conditional mutagenesis experiments are that while the *Zic4* lineage astroglia do require *Ext1* to form midline astroglial structures they do not require *Hs2st*, strongly suggesting that while these *Zic4* lineage cells require HS on their cell surface to respond to translocation signals there is no need for the HS to be 2-O sulphated. In contrast *Hs2st* is absolutely required in the surrounding *Emx1* lineage cells indicating a non cell autonomous mechanism by which 2-O HS sulphation controls the transmission of translocation signals to the *Zic4* lineage astroglial precursors.

***Hs2st* is not required cell autonomously by CC axons to navigate the midline.**

The conditional mutagenesis experiments showed that Hs2st has a non cell autonomous role in GW→IG somal translocation, but, because Hs2st is expressed throughout the cerebral cortex, did not resolve whether there is an additional cell autonomous requirement in CC axon navigation. To answer this we performed *ex vivo* transplant experiments in which cerebral cortical tissue from transgenic mice ubiquitously expressing τ GFP, which efficiently labels axons of τ GFP⁺ cells, was transplanted into τ GFP⁺ telencephalic slices containing the CC axon pathway and CSB structures (Niquille et al., 2009; Pratt et al., 2000). When *wild-type* (WT) E17.5 τ GFP⁺ cortical explants are transplanted into age matched τ GFP⁺ WT cortical slices τ GFP⁺ axons extend across the telencephalic midline forming the characteristic U-shape of the CC and reach the cortex of the opposite hemisphere (n=3/3 cultures, arrows in Fig 6A,D point to crossing axons). When *Hs2st*^{-/-} τ GFP⁺ cortical explants are transplanted into τ GFP⁺ WT slices, axons are able to cross the midline to reach the opposite hemisphere in a manner indistinguishable from that seen in the WT→WT transplants (n=4/4 cultures, arrows in Fig 6B,E point to crossing axons). In contrast, when τ GFP⁺ WT cortical explants are transplanted into τ GFP⁺ *Hs2st*^{-/-} slices axons are unable to reach the opposite cortical hemisphere and instead remain within the cingulate cortex or invade the septum (n=6/6 cultures), resembling the *in vivo* CC phenotype observed

in *Hs2st*^{-/-} embryos (Clegg et al., 2014; Conway et al., 2011). Note that in all cultures a few axons grew into the septum (arrowheads in Fig 6 D,E,F). Schematics summarising these experiments are shown in Fig 6 G,H,I. These data show 2-O HS sulphation is not required cell autonomously by CC projection neurons for axon guidance across the midline strongly suggesting that disorganisation of midline guidepost astroglial cells is the primary cause of the *Hs2st*^{-/-} CC agenesis phenotype.

Abnormally high FGF/ERK signalling causes the *Hs2st*^{-/-} precocious astroglial translocation phenotype.

We previously reported a correlation between hyperactive ERK signalling at the CSB and precocious somal translocation of astroglia to the midline in *Hs2st*^{-/-} embryos but we did not formally establish that this stemmed from hyperactive FGF/ERK signalling (Chan et al., 2017; Clegg et al., 2014). To address this we employed an *ex vivo* assay in which coronal *WT* or *Hs2st*^{-/-} telencephalic slices incorporating the CSB were cultured on floating membranes for long enough to allow somal translocation to the midline and attempted to rescue the *Hs2st*^{-/-} phenotype by pharmacological abrogation of FGF/ERK signalling. *WT* or *Hs2st*^{-/-} E14.5 slices were cultured in the presence of the Fgfr1 inhibitor SU5402 dissolved in DMSO (FGFi treatment) to inhibit FGF/ERK signalling or in DMSO alone (untreated control) for 48hr (Fig 7A). To aid subsequent identification of translocating cells, a subpopulation RGCs undergoing S-phase in the VZ at E14.5 were labelled just prior to culturing with a single pulse of BrdU. Immunohistochemistry for pErk (brown stain in Fig 7 B,D,F,H) confirms inhibition of FGF/ERK signalling in both FGFi treated *WT* and *Hs2st*^{-/-} cultures (Fig 7D,H) compared to untreated cultures (Fig 7B,F) showing that FGF signalling through Fgfr1 accounts for ERK phosphorylation in both genotypes so, importantly, demonstrating that ERK hyperactivation in *Hs2st*^{-/-} embryos does not stem from an FGF-independent mechanism for ERK activation (Chan et al., 2017; Clegg et al., 2014). After 48 hours some Sox9⁺ cells (red) had left the VZ and translocated to the midline in untreated *WT* cultures (arrow in Fig 7C) with many more populating the midline in untreated *Hs2st*^{-/-} cultures (arrow in Fig 7G) validating that our *ex vivo* assay replicates the *in vivo* *Hs2st*^{-/-} phenotype. Consistent with our hypothesis, FGFi treatment of both *WT* and *Hs2st*^{-/-} cultures resulted in a large decrease in Sox9⁺ cells reaching the midline (compare Fig 7E,I to C,G). We quantified glial translocation by counting the numbers of Sox9⁺ cells born in the VZ at E14.5 (Sox9⁺;BrdU⁺ cells, yellow – inset in Fig 7 C,E,G,I shows higher magnification) that had exited the VZ towards the midline (VZ demarcated by dotted line in Fig 7 C,E,G,I) after 2 days in culture. Counts of

BrdU⁺;Sox9⁺ cells showed that glial translocation was significantly greater in *Hs2st*^{-/-} compared to *WT* cultures along the rostro-caudal axis (dark purple and green lines in Fig 7J) and in both cases almost completely suppressed by FGF_i treatment (pale purple and green lines in Fig 7J).

We conclude that the precocious glial translocation phenotype in *Hs2st*^{-/-} embryos is caused by hyperactive FGF/ERK signalling from E14.5 onwards. Taken together with our *Hs2st* conditional mutagenesis experiments demonstrating a non cell autonomous role for *Hs2st* in astroglial precursor translocation we hypothesise that *Hs2st* normally suppresses the supply of FGF proteins to translocation competent astroglial precursors in the GW.

***Hs2st* suppresses Fgf17 protein levels.**

We next sought to identify an FGF protein that is targeted by *Hs2st*. Despite its well known role in CC development Fgf8 protein levels are not significantly increased at the CSB of *Hs2st*^{-/-} embryos forcing us to consider other FGFs (Chan et al., 2017; Clegg et al., 2014). A promising candidate is *Fgf17*, a member of the *Fgf8* subfamily transcribed at the CSB in a similar pattern to *Fgf8* (Cholfin and Rubenstein, 2008; Zhang et al., 2012b). Fgf17 is a canonical FGF that binds to HS, so is potentially regulated via its interaction with HS, and is known to play a role in patterning the telencephalon although its role in CC development has not been fully characterised (Cholfin and Rubenstein, 2007; Hoch et al., 2015; Li and Kusche-Gullberg, 2016). We hypothesised that *Hs2st* normally suppresses Fgf17 protein and predicted that Fgf17 protein levels would be increased at the *Hs2st*^{-/-} CSB. We compared the expression of Fgf17 protein in the developing CSB of *WT* and *Hs2st*^{-/-} embryos at three developmental stages (E12.5, E14.5, and E16.5), spanning the interval of midline glial translocation (Fig 8A_{1,2}-H_{1,2}). At E12.5 telencephalic Fgf17 protein is restricted to the CSB region with no obvious difference between *WT* and *Hs2st*^{-/-} (compare Fig 8 A₁,B₁ to A₂,B₂). By E14.5 there is an expanded Fgf17 protein domain at the CSB of *Hs2st*^{-/-} embryos (compare Fig 8 D₁,E₁ to D₂,E₂, * in E₂ marks the expanded Fgf17 protein domain). Quantification of Fgf17 immunofluorescence shows a significant ~2 fold increase in Fgf17 protein levels in this region of *Hs2st*^{-/-} CSB (Fig 8W – compare blue and green bars). At E16.5 Fgf17 protein is much closer to detection threshold than at the earlier stages in both genotypes (Fig 8G_{1,2},H_{1,2}) although the increased protein spread in the mutant persists (* in Fig 8H₂) indicating that the *Hs2st*^{-/-} CSB is exposed to a prolonged overdose of Fgf17 protein spanning E14.5-E16.5. We next examined *Fgf17* mRNA at the CSB so see whether the

502 increase in Fgf17 protein in *Hs2st*^{-/-} CSB was underpinned by altered *Fgf17* gene expression.
 503 There was no evidence for this at E12.5 or E14.5 where *Fgf17* mRNA expression pattern
 504 remains similar between *Hs2st*^{+/+} and *Hs2st*^{-/-} embryos (compare Fig 8 C₁ to C₂ and F₁ to F₂),
 505 however, the expression domain of *Fgf17* mRNA is increased in E16.5 *Hs2st*^{-/-} CSB
 506 (compare Fig 8I₁ to I₂, * in I₂ marks expanded *Fgf17* mRNA domain). This subsequent
 507 increase in *Fgf17* mRNA in the E16.5 *Hs2st*^{-/-} CSB indicates that the *Hs2st*^{-/-} phenotype has a
 508 transcriptional component or that there are more cells expressing *Fgf17* mRNA in the
 509 expanded *Hs2st*^{-/-} IG although this cannot be the primary event as it is not apparent at E14.5,
 510 the stage at which we previously identified precocious astroglial precursor translocation was
 511 well underway in *Hs2st*^{-/-} embryos (Clegg et al., 2014).

512 Mosaic analysis (Fig 5) indicated that *Hs2st* function in the *Emx1* lineage negatively
 513 regulates a signal promoting GW→IG translocation of *Zic4* lineage glial cells by a non cell
 514 autonomous mechanism and Fgf17 expression analysis (Fig 8) makes Fgf17 a strong
 515 candidate for the signal. Based on this we hypothesised that Fgf17 is expressed in cells
 516 surrounding the *Zic4* lineage cells and performed detection of *Fgf17* mRNA or protein in
 517 E14.5 WT embryos in which the *Zic4* lineage is labelled GFP⁺. *Fgf17* mRNA is expressed at
 518 the GW and the IG (Fig 8J) and higher power magnification shows that in the VZ GFP⁺ cells
 519 express little if any *Fgf17* mRNA and conversely cells expressing the highest levels of *Fgf17*
 520 mRNA are GFP⁻ (Fig 8 K₁₋₃, arrows indicate GFP⁺ cell location). This complementarity
 521 between Fgf17 mRNA expressing and *Zic4* lineage cells is preserved at the IG (Fig 8L₁₋₃,
 522 arrows indicate GFP⁺ cell location). Fgf17 protein predominates at the IG (Fig 8M) and
 523 higher power magnification shows that while Fgf17 protein is barely detectable at the GW
 524 (Fig 8N₁₋₃) there are a number of much higher Fgf17 expressing cells at the IG and these cells
 525 are GFP⁻ confirming that they do not belong to the *Zic4* lineage (Fig 8O₁₋₃, arrows indicate
 526 GFP⁺ cell location). Interestingly, although cells in the GW and IG express comparable levels
 527 of *Fgf17* mRNA (compare Fig 8K₁ to L₁) the expression of Fgf17 protein is much higher in
 528 the IG (compare Fig 8N₁ to O₁) suggesting a post-transcriptional repression selectively at the
 529 GW. Our identification of Hs2st as a repressor of Fgf17 protein levels at this stage makes
 530 Hs2st a strong candidate, indeed, closer examination of *Hs2st* expression using the *Hs2st*-
 531 *LacZ* reporter shows that Hs2st is expressed in a GW^{High}-IG^{Low} pattern (Fig 8P, also apparent
 532 in the Hs2st immunohistochemistry (Fig 1B)), complementary to the GW^{Low}-IG^{High} Fgf17
 533 protein distribution. Together these data bolster the idea that Hs2st acts to suppress Fgf17
 534 protein supply to *Zic4* lineage cells by a post-transcriptional mechanism.

We conclude that *Hs2st* primarily suppresses the level and spread of Fgf17 protein emanating from the *Emx1* lineage in the CSB.

***Hs6st1* does not affect Fgf17 protein levels.**

We next addressed whether the ability of 2-O HS sulphation to suppress Fgf17 protein levels *in vivo* represented a specific function of *Hs2st* or was redundant with other HSTs. We chose to examine *Hs6st1*, an HST that catalyses 6-O HS sulphation, because we have previously shown that *Hs6st1* (but not *Hs2st*) suppresses levels of the closely related Fgf8 protein at the CSB *in vivo* (Chan et al., 2017; Clegg et al., 2014). However, we were unable to detect increased expression of Fgf17 protein (compare Fig 8 Q₁, R₁ to Q₂, R₂ and T₁, U₁ to T₂, U₂) or *Fgf17* mRNA (compare Fig 8 S₁ to S₂ and V₁ to V₂) in *Hs6st1*^{-/-} compared to wild-type CSB at either E14.5 or E16.5. Quantification of Fgf17 immunofluorescence shows unchanged Fgf17 protein levels in this region of *Hs6st1*^{-/-} CSB (Fig 8W – compare blue and purple bars). These data demonstrate that the negative relationship between *Hs2st* and *Fgf17* is selective *in vivo* because it does not apply to *Hs6st1*.

Exogenously applied Fgf17 phenocopies the *Hs2st*^{-/-} astroglial translocation phenotype.

Our data suggest that the *Hs2st*^{-/-} phenotype stems from abnormally high levels of Fgf17 protein at the CSB causing FGF/ERK hyperactivation and precocious somal translocation to the IG. This requires that *Hs2st*^{-/-} CSB cells are competent to respond to Fgf17 protein and that application of ectopic Fgf17 triggers precocious glial translocation, neither of which have been previously established. We redeployed the CSB *ex vivo* culture assay (see Fig 7) with the modification that beads soaked in either recombinant Fgf17 protein (Fgf17 treatment) or in BSA (control) were implanted into coronal slices of CSB region on either side of the midline (Fig 9A). *WT* or *Hs2st*^{-/-} slices implanted with Fgf17 and BSA beads were cultured for 2 hours before processing for Fgf17 (green signal) and pErk (red signal) double immunofluorescence (Fig 9B). In both *WT* and *Hs2st*^{-/-} cultures Fgf17 protein was detectable adjacent to the edge of the bead (green signal) and this activated ERK phosphorylation in a similar pattern (red signal) with no obvious differences between *WT* and *Hs2st*^{-/-} indicating that *Hs2st*^{-/-} CSB tissue is competent to respond to Fgf17 (Fig. 9B top row). The lack of Fgf17 or pERK signal in the BSA control (Fig 9B, bottom row) confirms Fgf17 antibody specificity and that pERK activation was specifically induced by exogenously applied Fgf17. We performed Sox9/BrdU analysis (exactly as described above for the FGF experiments - Fig 7) to assess the impact of experimentally introduced Fgf17 on astroglial

translocation to the midline after 48 hours in culture. The results were dramatic, the side with the Fgf17-bead showed many more Sox9⁺ (red) cells in the IG region (large arrow on right side of Fig 9C) than the side with the BSA bead (smaller arrow on left side of Fig9C). Quantification of Sox9⁺;BrdU⁺ (yellow) cells (Fig 9D shows higher magnification of IG region) confirmed a significant increase in astroglial translocation to the midline along the rostro-caudal axis on the side exposed to Fgf17 (Fig 9E, compare green (Fgf17) to black (control) lines). An important function of IG glia is to secrete Slit2 and repulsively guide CC axons in the correct trajectory across the midline. At E16.5 *Slit2* mRNA is normally expressed in the IG region and in *Hs2st*^{-/-} embryos the midline *Slit2* expression domain is expanded (compare Fig 2C,E to D,F – *Slit2* expression domain bracketed). Experimentally introduced Fgf17 is sufficient to phenocopy this aspect of the *Hs2st*^{-/-} phenotype in our *ex vivo* assay as the side exposed to the Fgf17 bead has a much larger *Slit2* domain than the BSA treated side (compare left (Fgf17) and right (control) bracketed areas in Fig 9F) consistent with precocious translocation of excessive numbers of *Slit2*⁺ IG glia.

We conclude that *Hs2st*^{-/-} CSB tissue is competent to respond to Fgf17 protein and abnormally high levels of Fgf17 protein are sufficient to phenocopy the *Hs2st*^{-/-} astroglial translocation phenotype consistent with the model presented in Fig 10.

***Hs2st* selectively facilitates physical interaction between Fgf17 protein and HS.**

Our *in vivo* data show that *Hs2st* suppresses the levels of Fgf17 protein and that this represents a selective interaction between *Hs2st* mediated 2-O HS sulphation and Fgf17 protein levels *in vivo* because *Hs2st* does not suppress the levels of the closely related Fgf8 protein while *Hs6st1*, which catalyses 6-O HS sulphation, does not suppress Fgf17 protein levels (Chan et al., 2017; Clegg et al., 2014), Fig 8). These *in vivo* experiments do not however resolve whether differential sulphation has a correspondingly direct selective effect on the physical interaction between HS and Fgf17. In order to test the hypothesis that *Hs2st* has a selective effect on the binding of Fgf17 protein to HS molecules we turned to a biochemical assay, the ligand and carbohydrate engagement (LACE) assay, that probes physical interaction between HS and FGF proteins by quantifying the ability of endogenous HS in tissue sections to form Fgf:Fgfr:HS complexes with exogenously added Fgf protein and Fgfr ectodomain fused to an Fc tag for immunofluorescent detection (Allen et al., 2001; Chan et al., 2015). We used the Fgf17:Fgfr1 LACE assay to compare the binding of Fgf17 protein to HS in *WT*, *Hs2st*^{-/-} and *Hs6st1*^{-/-} CSB tissue at E14.5 and E16.5 in order to test the hypothesis that Fgf17:HS physical interaction is selectively sensitive to loss of 2-O HS

603 sulphation in *Hs2st*^{-/-} tissue (Fig 11 A-J, O). We used the Fgf8:Fgfr3 LACE assay to compare
 604 the binding of Fgf8 protein to HS in *WT* and *Hs2st*^{-/-} CSB tissue at E14.5 and E16.5 to test the
 605 hypothesis that the Fgf8:HS physical interaction is insensitive to loss of 2-O HS sulphation in
 606 *Hs2st*^{-/-} tissue (Fig 11 K-N, P).

607 In both E14.5 and E16.5 *WT* tissue the Fgf17:Fgfr1 and Fgf8:Fgfr3 LACE assays
 608 produced a strong LACE signal (Fig 11 A,F,K with higher magnification of boxed areas
 609 enclosing CSB region shown in A', F', K'). Control experiments show this LACE signal was
 610 drastically reduced by pre-treating the tissue with heparinitase to digest HS (Fig 11 D,I,M,
 611 with higher magnification of CSB in D', I', M') or omitting Fgf17 or Fgf8 protein from the
 612 assay (Fig 11 E,J,N with higher magnification of CSB in E', J', N'). Together these controls
 613 confirm the LACE signal provides a specific readout of the interaction between each FGF
 614 protein and HS molecules. To determine the effect of differential sulphation on the physical
 615 interaction between HS and Fgf8 or Fgf17 we examined how the LACE signal was affected
 616 when the assay was performed on *Hs2st*^{-/-} and *Hs6st1*^{-/-} tissue. As predicted by our hypothesis
 617 the binding of Fgf17 to HS is selectively sensitive to 2-O HS sulphation as we found that the
 618 Fgf17:Fgfr1 LACE signal was much weaker than *WT* in *Hs2st*^{-/-} tissue (compare B,B',G,G' to
 619 A,A',F,F') but similar to *WT* in *Hs6st1*^{-/-} tissue (compare C,C',H,H' to A,A',F,F').
 620 Quantification of Fgf17:Fgfr1 LACE signal intensity in Fig 11 O shows a significant ~4-fold
 621 reduction in *Hs2st*^{-/-} (green bar) compared to *WT* (blue bar) but no significant difference to
 622 *WT* in *Hs6st1*^{-/-} (purple bar). As predicted by our hypothesis that the binding of Fgf8 to HS is
 623 not sensitive to 2-O HS sulphation we found that there was no difference in the Fgf8:Fgfr3
 624 LACE signal between *WT* and *Hs2st*^{-/-} tissue (compare Fig 11 K,K' to L,L'). Quantification
 625 of Fgf8:Fgfr3 LACE signal intensity in Fig 11 P shows no significant difference between
 626 *Hs2st*^{-/-} (green bar) compared to *WT* (blue bar). These LACE results are summarised
 627 schematically in Fig 11Q which shows that of the five *HST* genotype and FGF ligand
 628 permutations tested only the Fgf17:HS physical interaction is sensitive to *Hs2st* genotype, as
 629 predicted by the hypothesis that 2-O HS sulphation has a specific effect on the ability of HS
 630 to bind Fgf17.

631 Discussion

632 Embryonic corpus callosum (CC) development involves multiple cell and molecular
 633 events that ultimately guide callosal axons across the telencephalic midline to connect with
 634 their synaptic targets in the contralateral hemisphere. Three subpopulations of midline
 635 astroglia play pivotal roles in guiding callosal axons across the telencephalic midline. Midline
 636

zipper (MZ) glia facilitate fusion of the cerebral hemispheres and provide a substrate for crossing callosal axons while *Slit2*⁺ indusium griseum (IG) and glial wedge (GW) astroglia channel crossing axons into the correct path by Robo/Slit mediated chemorepulsion (Bagri et al., 2002; Gobius et al., 2016; Shu and Richards, 2001; Shu et al., 2003). These astroglial populations originate from RGCs born in the VZ of the septal midline and either remain in the VZ at the glial wedge (GW astroglia) or translocate in response to FGF signals, of which Fgf8 appears to be particularly important, to the pial surface of the telencephalic midline (MZ and IG astroglia) (Clegg et al., 2014; Gobius et al., 2016; Moldrich et al., 2010; Smith et al., 2006). Both *Slit2*⁺ IG and *Slit2*⁻ MZ astroglia are essential for CC development and both these astroglial populations originate from the septal VZ *Zic4* lineage so the lack of an overt CC phenotype in *Hs2st*^{F/FI};*Zic4*^{Cre} embryos following conditional knockout of *Hs2st* in the *Zic4* lineage indicates that neither MZ or IG astroglial precursors have a cell autonomous requirement for *Hs2st* to translocate in appropriate numbers. In *Hs2st*^{-/-} embryos there is an expansion of the *Slit2* expression domain at the CSB pial surface coinciding with increased Sox9⁺ glial cells and this is phenocopied by application of exogenous Fgf17 to *Hs2st*^{+/+} CSB *ex vivo* strongly suggesting increased numbers of *Slit2*⁺ glial cells at the midline reflect excessive GW→IG somal translocation enlarging the IG (current study). We cannot rule out the possibility that disrupted MZ glial translocation also contributes to the *Hs2st*^{-/-} phenotype although this would not alter our conclusion that *Hs2st* plays a non-cell autonomous role in the *Zic4*-lineage astroglial translocation phenotype. Our model (Fig 10) posits that ectopic *Slit2*⁺ astroglia at the midline block the transit of CC axons. In principle this could be tested by rescuing the CC axon midline crossing in *Hs2st*^{-/-};*Slit2*^{-/-} embryos (along similar lines to the *Slit2* genetic rescue of the *Hs6st1*^{-/-} phenotype we reported in *Hs6st1*^{-/-};*Slit2*^{-/-} embryos (Conway et al., 2011)). However, in contrast to the fully penetrant (100%) *Hs6st1*^{-/-} CC phenotype, the partial penetrance (~50%) of the *Hs2st*^{-/-} CC phenotype introduces a confounding factor of distinguishing ‘rescued’ from ‘unaffected’ *Hs2st*^{-/-} embryos, a problem that would be compounded if only a proportion of embryos destined to be ‘affected’ were rescued (see (Clegg et al., 2014; Conway et al., 2011)) so a prohibitively large number of animals would be required to demonstrate a statistically significant rescue.

Eliminating HS (*Ext1* mutagenesis) compared to 2-O HS sulphation (*Hs2st* mutagenesis) from the same cell lineages allowed us to distinguish physiological functions generally attributable to HS from those specifically requiring 2-O HS sulphation by comparing the *Ext1* and *Hs2st* phenotypes. We found that while *Zic4* lineage cells were unable to support CC development when they lacked HS (*Zic4*^{Cre};*Ext1*^{F/FI} embryos) there

671 was no similar requirement for 2-O HS sulphation in the *Zic4* lineage (*Zic4*^{Cre};*Hs2st*^{Fl/Fl}
 672 embryos) indicating that *Zic4* lineage cells require HS but that 2-O HS sulphation is
 673 dispensable for their contribution to CC development, specifically the ability of astroglial
 674 precursors to cell autonomously sense translocation signals. We found that HS and 2-O HS
 675 sulphation are both required in the *Emx1* lineage (*Emx1*^{CreER};*Ext1*^{Fl/Fl} and
 676 *Emx1*^{CreER};*Hs2st*^{Fl/Fl} embryos) although the axonal and astroglial phenotypes were not
 677 identical. Somewhat counterintuitively, removing HS completely from the *Emx1* lineage in
 678 *Emx1*^{CreER};*Ext1*^{Fl/Fl} embryos had a less severe effect on the distribution of GFAP⁺ midline
 679 glia than preserving HS but blocking its 2-O sulphation, as the accumulation of astroglia at
 680 the pial surface of the midline was much more pronounced in *Emx1*^{CreER};*Hs2st*^{Fl/Fl} embryos.
 681 We speculate that completely removing HS from the *Emx1* lineage results in a general
 682 destabilisation of FGF protein gradients so mitigating precocious somal translocation by *Zic4*
 683 lineage astroglial precursors (Chan et al., 2017; Qu et al., 2011; Qu et al., 2012; Shimokawa
 684 et al., 2011). The relatively normal midline astroglial organisation in *Emx1*^{CreER};*Ext1*^{Fl/Fl}
 685 embryos poses the question of whether glial disorganisation is a major contributor to their CC
 686 agenesis phenotype. In *Emx1*^{CreER};*Hs2st*^{Fl/Fl} embryos the Probst bundles form right next to the
 687 midline, consistent with our hypothesis that ectopic Slit2⁺ astroglia at the midline are
 688 repelling CC axons from crossing the midline (Conway et al., 2011) & current study). In
 689 contrast the Probst bundles in *Emx1*^{CreER};*Ext1*^{Fl/Fl} embryos form much more lateral to the
 690 midline at some distance from the IG indicating CC axons are misrouted at an earlier stage of
 691 their navigation than in *Emx1*^{CreER};*Hs2st*^{Fl/Fl} embryos. HS is required cell autonomously for
 692 navigating axons to respond to axon guidance molecules, including Netrin1 and Slit2
 693 (Matsumoto et al., 2007; Piper et al., 2006). A plausible explanation is that in
 694 *Emx1*^{CreER};*Ext1*^{Fl/Fl} embryos the *Emx1* lineage HS-deficient CC axons cannot respond
 695 appropriately to guidance cues that would normally guide them towards the midline and are
 696 already misrouted before they come under the influence of the midline astroglia In contrast
 697 *Hs2st*^{-/-} CC axons express HS lacking 2-O sulphation that does not affect their ability to
 698 respond to guidance cues (current study) so they reach the midline but are prevented from
 699 crossing by the ectopic Slit2⁺ glia in the expanded IG.

700 Biochemical (LACE) data shows that physical interaction between Fgf17 and HS is
 701 facilitated by Hs2st (but not Hs6st1) and that Hs2st facilitates physical interaction between
 702 HS and Fgf17 (but not Fgf8) suggesting a molecular mechanism underpinning Hs2st
 703 selectively suppressing levels of Fgf17 *in vivo* (Allen and Rapraeger, 2003; Chan et al., 2015;
 704 Chan et al., 2017; Clegg et al., 2014), current study). We speculate that Hs2st exerts its

selective effect on Fgf17 protein levels because HS lacking 2-O HS sulphation has reduced affinity for Fgf17 (but not Fgf8) so increasing the half-life of Fgf17 (but not Fgf8) in the ECM by selectively reducing the rate that Fgf17 protein is cleared by HS-mediated receptor mediated endocytosis of canonical FGFs while leaving Fgf8 unaffected (Yu et al., 2009). Our conditional mutagenesis experiments clearly demonstrate there is no cell autonomous requirement for *Hs2st* in astroglial precursor translocation in *Emx1^{CreER};Hs2st^{Fl/Fl}* embryos, however the reduced efficiency of HS:Fgf17:Fgfr1 complex formation in the LACE assay implies that *Hs2st* might also play a cell-autonomous role in the response to Fgf17 protein. We speculate that even if *Hs2st*^{-/-} astroglial precursors are less sensitive to Fgf17 than their wild-type counterparts their translocation to the midline is primarily driven by Fgf8 so is not significantly affected in *Zic4^{Cre};Hs2st^{Fl/Fl}* embryos. A putative reduced sensitivity of *Hs2st*^{-/-} astroglial precursor cells to Fgf17 also begs the question of how elevated Fgf17 could trigger precocious glial translocation in *Hs2st*^{-/-} embryos. The Fgf17 bead assay experiment shows that *Hs2st*^{-/-} cells retain competence to respond to Fgf17 by phosphorylating ERK and LACE data shows that HS devoid of 2-O HS sulphation still interacts with Fgf17 albeit with reduced efficiency. The explanation that best fits our experimental data, therefore, is that increased Fgf17 protein levels in *Hs2st*^{-/-} embryos overrides any reduction in competency of *Hs2st*^{-/-} cells to respond to Fgf17 protein and the net effect is elevated FGF/ERK signalling and consequent precocious astroglial translocation.

This study makes two major novel contributions to our understanding of the cell and molecular roles of differential HS sulphation in the regulation of forebrain development. First that a primary cellular role of 2-O HS sulphation *in vivo* is not to modulate the competence of astroglial precursor cells to respond to translocation signals by a cell autonomous mechanism (as would be predicted by the classic role for HS in modulating the formation of the FGF:FGFR:HS receptor complex on the surface of responding cells) but instead to regulate the supply of translocation signals to astroglial precursors by a non cell autonomous mechanism. Second that the interaction between 2-O sulphated HS and Fgf17 protein is selective because it does not apply to the closely related Fgf8 protein or to 6-O HS sulphation catalysed by Hs6st1. The most parsimonious explanation linking these cell and molecular events is that higher than normal levels of Fgf17 protein at the CSB of *Hs2st*^{-/-} embryos causes the precocious astroglial precursor translocation phenotype and subsequent misrouting of CC axons (Fig 10). Our rescue of the *Hs2st*^{-/-} precocious astroglial precursor translocation phenotype *ex vivo* by generic pharmacological inhibition of FGF signalling with SU5402 directly supports the hypothesis that hyperactive FGF/ERK signalling causes the phenotype.

739 Given the well known role of FGF/ERK signalling in triggering astroglial precursor
 740 translocation to the IG, our findings that exogenously applied Fgf17 protein is sufficient to
 741 phenocopy the *Hs2st*^{-/-} astroglial precursor translocation phenotype, and that *Hs2st*^{-/-} CSB
 742 cells activate ERK in response to Fgf17 protein, it is extremely unlikely that increased Fgf17
 743 protein levels *in vivo* wouldn't result in ERK hyperactivation and consequent precocious
 744 astroglial precursor translocation in *Hs2st*^{-/-} embryos. However, the current study does not
 745 provide formal proof that the elevated levels of Fgf17 protein are solely responsible for the
 746 FGF/ERK hyperactivation or precocious astroglial precursor translocation phenotypes in
 747 *Hs2st*^{-/-} embryos and we were unable to design an experiment that could further discriminate
 748 between the functions of Fgf17 and Fgf8 and directly test functional selectivity of Hs2st for
 749 Fgf17 in this context. We considered employing a classic rescue experiment strategy by
 750 genetically reducing *Fgf17* dosage in *Hs2st*^{-/-} embryos (*Fgf17*^{-/-};*Hs2st*^{-/-} rescue) but on
 751 balance elected not to because at best it would provide equivocal evidence either for or
 752 against the hypothesis that 2-O sulphated HS interacts selectively with Fgf17 protein.
 753 FGF/ERK hyperactivation caused by overexpression of a particular FGF protein can be
 754 rescued by any experimental manipulation that restores ERK signalling to normal levels and
 755 not uniquely by restoring the levels of the FGF protein that underpins the phenotype.
 756 Specifically, reducing *Fgf17* dosage could elicit a rescue of ERK hyperactivation and
 757 collateral phenotypes at the *Hs2st*^{-/-} CSB by reducing FGF/ERK signalling output whether or
 758 not abnormally high Fgf17 bioavailability was the primary cause. Analogously we interpret
 759 rescue of the *Hs6st1*^{-/-} precocious astroglial precursor translocation phenotype in *Hs6st1*^{-/-}
 760 *;Fgf8*^{neo/neo} embryos as evidence that *Hs6st1* normally acts to keep FGF/ERK signalling in
 761 check rather than as evidence for a selective genetic interaction between *Fgf8* and *Hs6st1*
 762 (Clegg et al., 2014). Conversely, failure to rescue the *Hs2st*^{-/-} phenotype in *Fgf17*^{-/-};*Hs2st*^{-/-}
 763 embryos (or using other methods to reduce Fgf17 protein levels or functionality) would not
 764 falsify the hypothesis that increased Fgf17 bioavailability caused the *Hs2st*^{-/-} phenotype
 765 because there are several alternative explanations. When we employed a similar strategy in a
 766 similar context to rescue the *Hs6st1*^{-/-} astroglial precursor precocious translocation phenotype
 767 by genetically reducing *Fgf8* dosage the rescue was only successful in a minority of isogenic
 768 *Hs6st1*^{-/-};*Fgf8*^{neo/neo} embryos and a likely explanation is that compensatory mechanisms act
 769 when *Fgf* gene dosage is manipulated (Clegg et al., 2014). Such compensation will generate
 770 false negative results making it unsafe to interpret unrescued *Fgf17*^{-/-};*Hs2st*^{-/-} embryos as
 771 falsifying the hypothesis that the phenotype is underpinned by excess Fgf17 protein. There
 772 are additional technical confounds that could lead to false negatives because a rescue likely

requires precise restoration of normal Fgf17 protein levels (so no rescue could reflect technical failure to restore Fgf17 protein levels to normal) and in any case the CC phenotype of *Fgf17*^{-/-} embryos has not been thoroughly characterised so *Hs2st*^{-/-};*Fgf17*^{-/-} phenotypes may well be problematic to interpret (Cholfin and Rubenstein, 2007, 2008). In addition to not being decisive for or against selectivity we note that demonstrating genetic interaction between *Hs2st* and *Fgf17* would not provide insight into whether the interaction was molecularly direct or not, in contrast to biochemical LACE data we present in the current study.

The closely related ‘Fgf8 subfamily’ members *Fgf17* and *Fgf8* are both transcribed by cells in the CSB region yet have different roles in forebrain development with available evidence, while not ruling out a role for *Fgf17*, suggesting that *Fgf8* is the primary driver of astroglial precursor translocation required for CC development (Cholfin and Rubenstein, 2007, 2008; Gobius et al., 2016; Moldrich et al., 2010; Toyoda et al., 2011). The independent suppression of Fgf17 and Fgf8 protein levels by HS modified by *Hs2st* and *Hs6st1* respectively may have facilitated the evolution of this system by providing a mechanism to tilt the Fgf17:Fgf8 protein balance to give Fgf8 the more dominant role in regulating astroglial precursor translocation (Chan et al., 2017; Clegg et al., 2014), Current study). In this sense there are parallels to other negative regulatory strategies, for example micro-RNAs that function by protecting cells from the expression of particular proteins that would be detrimental if expressed.

Figure Legends:

Figure 1. Hs2st protein is expressed in the cerebral cortex and the septum during CC formation. (A) Immunohistochemistry for Hs2st at E14.5 (B-D) Higher magnification shows punctate subcellular Hs2st expression (inset, B) Hs2st protein is expressed at the CSB (B), the VZ of the cortex (C) and the cortical plate (D). (E) Immunohistochemistry for Hs2st at E18.5 (F-M) Hs2st protein is expressed in the IG (F), the GW (G), the septum (H), and the ventral telencephalon (I). Within the cortex Hs2st is expressed at the ventricular zone (J), the intermediate zone (K), Hs2st is not strongly expressed by the middle layers of the cortex (L), but is expressed by the deeper layers (M). (N-R) Hs2st antibody specificity. The Hs2st antibody produces signal in the GW (J,L), which is lost in *Hs2st*^{-/-} embryos (K,M). Western-blot performed on protein extracted from whole telencephalon using Hs2st antibody reveals the predicted ~42kDa band in WT extracts, which is lost in *Hs2st*^{-/-} extracts (N). B-D are

higher magnification images of boxed regions indicated in A. F-M are higher magnification images of boxed regions indicated in E. L and M are higher magnification images of boxed regions in J and K respectively. Insets in B, F, P and Q are higher magnification images of boxed regions. Scale bars: 500µm in A, 50µm in B-I, L, M; 100µm in J,K.

Figure 2. *Slit2* expression at the CSB of WT and *Hs2st*^{-/-} embryos at E16.5. (A, C, E) *In-situ* hybridisation for *Slit2* in WT embryos at 3 rostro-caudal positions labelling the GW and IG. (B, D, F) *In situ* hybridisation for *Slit2* in *Hs2st*^{-/-} embryos at equivalent positions to A, C and E respectively showing an expanded IG. Scale bar: 100µm in all panels.

Figure 3. *Emx1* and *Zic4* lineage contribution at the CSB. (A) *Zic4*^{cre} allele combined with a lox-stop GFP reporter has been used to label cell populations at E18.5. *Zic4*^{cre} labels cells of the septum. (B, C, D, E) *Zic4*^{cre} labels cells ventral to the CSB (dashed line, B,C) including *Sox9* expressing cells (arrowheads, C) but is not expressed by *Sox9* expressing cells dorsal to the CSB (arrows, C). *Zic4*^{cre} is expressed by IG glial cells (arrowheads, D) but not by surrounding cells. *Zic4*^{cre} is expressed by MZ glial cells (arrowheads, E). (F) Schematic of the *Zic4*^{cre} expressing cell lineage. (G) *Emx1*^{creER} allele combined with a lox-stop GFP reporter has been used to label cell populations at E18.5. *Emx1*^{creER} labels cells of the cortex. (H, I, J, K) *Emx1*^{creER} labels cells dorsal to the CSB (dashed line, H,I) including *Sox9* expressing cells (arrowheads, I) but is not expressed by *Sox9* expressing cells ventral to the CSB (arrows, I). *Emx1*^{creER} is not expressed by IG glial cells (arrows, J). *Emx1*^{creER} is not expressed by MZ glial cells (arrows, K). (L) Schematic of the *Emx1* expressing cell lineage. No phenotype was detected in *Hs2st*^{+/+} *Zic4*^{cre} or *Hs2st*^{+/+} *Emx1*^{creER} embryos (n=5 for each genotype). C, D and E are higher magnification images of the indicated regions in B. I, J and K are higher magnification images of the indicated regions in H. Scale bars: 500µm in A,G; 200µm in B and H; 50µm in C-E and I-K.

Figure 4. HS expression is required within both *Emx1* and *Zic4* lineage cells for CC formation. (A-I) Immunofluorescence for L1 (red) at E18.5 labels the CC while GFAP (green) labels glia. In control embryos the U-shaped CC has formed and is flanked by glia at the IG and GW (A, D, G). In *Ext1*^{fl/fl} *Emx1*^{creER} embryos CC axons do not cross the midline while glia at the IG and GW appear largely unaffected (B, E, H). In *Ext1*^{fl/fl} *Zic4*^{cre} embryos CC axon do not cross the midline while glia appear depleted at the IG and form abnormal bundles at the GW (C, F, I). (J-O) FGFR1/ FGF2 ligand and carbohydrate engagement

(LACE) assay is used to detect the presence of HS. In control embryos LACE signal can be seen throughout the telencephalon, and is of similar intensity within both the cortex and the septum (J, M). In *Ext1^{fl/fl} Emx1^{creER}* embryos LACE signal is significantly reduced within the cortex (K, N). In *Ext1^{fl/fl} Zic4^{cre}* embryos LACE signal is significantly reduced within the septum (L, O). D-I are higher magnification images of the indicated boxed regions in A-C, J-L are higher magnification images of the boxed region in G-I respectively. Scale Bars: 200µm in A-C and G-I; 100µm in D-F and J-L.

Figure 5. *Hs2st* expression is required within *Emx1* lineage cells but not *Zic4* lineage cells for CC formation. (A-C) Immunofluorescence for L1 and GFAP at E18.5. In control embryos the U-shaped CC has formed and the IG can be observed above the CC (A). In *Hs2st^{fl/fl} Zic4^{cre}* embryos the CC and IG form normally (B). In around half of *Hs2st^{fl/fl};Emx1^{creER}* embryos the CC fails to form, IG glia also extend ventrally (asterisks, C). In the remaining *Hs2st^{fl/fl};Emx1^{creER}* embryos the CC forms normally (C'). (D-I) Immunofluorescence for *Sox9* labels progenitor cells at the ventricular zone and mature glia at the IG, GFP labels cells in which cre is active. (D, G) In control (*Hs2st^{+/+};Emx1^{creER}*) embryos IG glia do not express GFP. (E, H) In *Hs2st^{fl/fl};Zic4^{cre}* embryos IG glia do express GFP and adopt their normal position. (F, I) In *Hs2st^{fl/fl};Emx1^{creER}* embryos GFP is expressed by cortical neurons and axons but not by abnormally positioned IG glia. (J-L) Immunohistochemistry for *Hs2st* shows expression of *Hs2st* in the IG. (J) in control embryos punctate *Hs2st* staining can be seen within IG cells. In *Hs2st^{fl/fl} Zic4^{cre}* embryos *Hs2st* is not expressed by IG glia (K). In *Hs2st^{fl/fl};Emx1^{creER}* embryos *Hs2st* is expressed by displaced glial cells (L). *Hs2st* immunohistochemistry in J-L was performed on adjacent tissue sections to those in D-I. (M) Quantification of *Sox9* expressing cell number at the IG in control (blue bar, n=4 embryos, 2 *Hs2st^{+/+};Zic4^{cre}* + 2 *Hs2st^{+/+};Emx1^{creER}*), affected *Hs2st^{fl/fl};Emx1^{creER}* (orange bar, n=4 embryos), and *Hs2st^{fl/fl};Zic4^{cre}* (purple bar, n=3 embryos). *Sox9⁺* numbers are significantly increased compared to control in *Hs2st^{fl/fl};Emx1^{creER}* embryos (* indicates p<0.05 on graph), (F(2, 7) = 42.16, p = 0.00013, ANOVA), post-hoc t-tests: control vs *Hs2st^{fl/fl};Emx1^{creER}* (t(4) = -8.08, p = 0.0013, t-test); & control vs *Hs2st^{fl/fl};Zic4^{cre}* (t(5) = 0.92, p = 0.40, t-test). Boxed regions in G-I are higher magnification images of boxed regions in D-F respectively. Insets in J, K and L are higher magnification images of boxed region shown on each image. Scale bars: 200µm in A-F; 100µm 50µm in G-I and J-L.

874 **Figure 6:** *Hs2st* is not required by CC axons in order to cross the telencephalic midline. (A,
875 D) After homotypic transplantation of E17.5 cortical explants from GFP⁺ control tissue into
876 the cortex of GFP⁻ control brain slices GFP⁺ CC axons are able to project across the midline
877 (arrows, D). (B, E) After transplantation of GFP⁺ *Hs2st*^{-/-} cortical explants into GFP⁻ control
878 brain slices GFP⁺ CC axons are able to project across the midline (arrows, E). (C, F) After
879 transplantation of cortical explants from GFP⁺ control tissue into the cortex of GFP⁻ *Hs2st*^{-/-}
880 brain slices GFP⁺ CC axons are unable to project across the midline and invade the septum.
881 Arrowheads indicate axons navigating into the septum in all conditions. (G-I) Schematic of
882 transplant experiments shown in A-C. D-F are higher magnification images of the boxed
883 region in A-C respectively. Scale bars: 200µm in all panels.

884
885 **Figure 7.** Hyperactive Fgf signalling causes precocious glia translocation in *Hs2st*^{-/-} CSB.
886 (A) Experimental outline of *Hs2st*^{-/-} phenotypic rescue experiment. Pregnant females were
887 injected at E14.5 with a BrdU pulse and CSB slices collected after 1 hour and cultured for
888 48hrs (B-I) *WT* or *Hs2st*^{-/-} CSB slices were cultured in the presence of either SU5402 (FGFi)
889 or DMSO (untreated vehicle control). (B, D, F, H) pErk immunohistochemistry shows that
890 FGF treatment reduces Fgf/ERK signalling. (C,E,G,I) Immunofluorescence for BrdU and
891 Sox9 in *WT* (C,E) and *Hs2st*^{-/-} (G,I) slices treated with FGF (E,I) or untreated (C,G), the
892 curved dotted line demarcates the basal edge of the VZ, arrows in C,G point to accumulations
893 of BrdU/Sox9⁺ cells at the midline (arrow size corresponds to cell number) with higher
894 magnification insets showing Sox9/BrdU⁺ (yellow) double labelled cells in IG region. (J)
895 Quantification of Sox9/BrdU⁺ double labelled cells in *WT* or *Hs2st*^{-/-} CSB slice cultures
896 treated with FGF or untreated (n=3 embryos for each condition). For both genotypes FGF
897 treatment significantly reduces the number of Sox9/BrdU⁺ cells that exit the VZ and moved
898 towards the IG at one or more rostro-caudal position (significant differences due to FGF
899 treatment within each genotype indicated on graph as **p<0.05 ***p<0.001). (F(3, 32) =
900 31.00, p = 0.0000000014, Two-way ANOVA) followed by t-test with Sidak's correction for
901 multiple comparisons at each position along the rostro-caudal axis. *WT* FGF vs *WT* untreated:
902 position 1 (t(16) = 1.67, p = 0.24, t-test); position 2 (t(16) = 2.37, p = 0.11, t-test); position 3
903 (t(16) = 2.25, p = 0.15, t-test); & position 4 (t(16) = 2.81, p = 0.050, t-test). *Hs2st*^{-/-} FGF vs
904 *Hs2st*^{-/-} untreated: position 1 (t(16) = 2.38, p = 0.11, t-test); position 2 (t(16) = 2.83, p =
905 0.048, t-test); position 3 (t(16) = 3.05, p = 0.030, t-test); & position 4 (t(16) = 4.60, p =
906 0.0012, t-test). Scale bars: 100µm B-I.

Figure 8. Expression of Fgf17 during CSB development in *WT* and *Hs2st*^{-/-} and *Hs6st1*^{-/-} embryos. **(A-C)** Fgf17 protein and mRNA expression at the E12.5 CSB of *WT* and *Hs2st*^{-/-} embryos. Fgf17 protein is expressed across the CSB in both *WT* and *Hs2st*^{-/-} embryos, with no obvious change in intensity or domain of expression. *Fgf17* mRNA expression overlaps well with the protein expression domain and is similar between *WT* and *Hs2st*^{-/-}. **(D-F)** Fgf17 protein and mRNA expression at the E14.5 CSB of *WT* and *Hs2st*^{-/-} embryos. Fgf17 protein is expressed at low levels at the CSB of *WT* embryos. In *Hs2st*^{-/-} embryos, the protein expression domain expands across the CSB (asterisks in E₂). *Fgf17* mRNA is unchanged at the CSB between *WT* and *Hs2st*^{-/-} embryos. **(G-I)** Fgf17 protein and mRNA expression at the E16.5 CSB of *WT* and *Hs2st*^{-/-} embryos. Fgf17 protein is expressed at low levels at the CSB of *WT* embryos (H₁). In *Hs2st*^{-/-} embryos, the protein expression domain expands (asterisks, H₂). There is a concurrent increase in *Fgf17* mRNA (asterisk, I₂). **(J-O)** Fgf17 mRNA (J, K_{1,2,3}, L_{1,2,3}) and Fgf17 protein (M, N_{1,2,3}, O_{1,2,3}) expression (red) relative to GFP⁺ *Zic4* lineage cells (indicated with white arrows) at the GW (K_{1,2,3}, N_{1,2,3}) and IG (L_{1,2,3}, O_{1,2,3}) of *WT* E14.5 embryos. **(P)** E14.5 expression of *Hs2st* by LacZ staining. *Hs2st* is expressed most highly at the VZ, with decreasing expression towards the pial surface. **(Q-V)** Fgf17 protein and mRNA expression at the E14.5 CSB of *WT* and *Hs6st1*^{-/-} embryos. Fgf17 protein is expressed at low levels at the CSB of *WT* embryos (Q₁, R₁). In *Hs6st1*^{-/-} embryos, the protein expression domain is similar to *WT* (Q₂, R₂). *Fgf17* mRNA expression is unchanged between *WT* and *Hs6st1*^{-/-} embryos (S₁, S₂). **(T-V)** Fgf17 protein and mRNA expression at the E16.5 CSB of *WT* and *Hs6st1*^{-/-} embryos. Fgf17 protein is expressed at very low levels at the CSB of both *WT* (T₁, U₁) and *Hs6st1*^{-/-} (T₂, U₂) embryos. *Fgf17* mRNA expression is unchanged between *WT* (V₁) and *Hs6st1*^{-/-} (V₂) embryos. **(W)** Quantification of Fgf17 immunofluorescence signal at CSB in *WT* (blue bar, n=3 embryos), *Hs2st*^{-/-} (green bar, n=3 embryos) and *Hs6st1*^{-/-} (purple bar, n=3 embryos). Fgf17 protein level is significantly increased compared to *WT* in *Hs2st*^{-/-} embryos (* indicates p<0.05 on graph), (F(2, 9) = 13.83, p = 0.0018, ANOVA), post-hoc t-tests: *WT* vs *Hs2st*^{-/-} (t(4) = -4.22, p = 0.014, t-test); & *WT* vs *Hs6st1*^{-/-} (t(6) = -0.98, p = 0.36, t-test). Boxed areas in A,D,G,Q,T shown at higher magnification in B,E,H,R,U respectively. Scale bars: 200μm in A,D,G,Q,T; 100μm in B,C,E,F,H,I,R,S,U,V,J,M,P; 10μm in K,L,N,O.

939 **Figure 9.** Fgf17-bead experiment. **(A)** Experimental outline of Fgf17 protein bead
 940 experiment in WT embryos. Pregnant females were injected at E14.5 with a BrdU pulse and
 941 CSB slices collected. One Fgf17 and one BSA bead were added to each side of the midline.
 942 **(B)** Fgf17 protein and pErk after 2 hours in culture. In both *WT* and *Hs2st*^{-/-} CSB slices, Fgf17
 943 and pErk are seen in tissue surrounding the Fgf17 bead. Staining for either is absent around
 944 the BSA bead (demarcated by dotted circle). **(C)** Immunofluorescence for BrdU and Sox9
 945 was performed on slices after 48 hours in culture, curved dotted lines indicate the basal edge
 946 of the VZ and straight dotted line indicates the midline. D shows a higher power of the
 947 arrowed regions in C. **(E)** Quantification of Sox9⁺/BrdU⁺ double labelled cells in CSB slice
 948 cultures with Fgf17 or BSA bead. The Fgf17 bead significantly increased the number of
 949 Sox9⁺/BrdU⁺ cells that exit the VZ and moved towards the IG (significant differences
 950 indicated on graph as **p<0.05 ***p<0.001) at the four caudal-most positions (n=5
 951 embryos). (F(1, 48) = 65.63, p = 0.000000000155, Two-way ANOVA) followed by t-test
 952 with Sidak's correction for multiple comparisons for Fgf17-bead vs BSA-bead at each
 953 rostral-caudal position: position 1 (t(48) = 1.45, p = 0.63, t-test); position 2 (t(48) = 2.36, p =
 954 0.13, t-test); position 3 (t(48) = 3.65, p = 0.0039, t-test); position 4 (t(48) = 4.47, p = 0.0003,
 955 t-test); position 5 (t(48) = 4.03, p = 0.0012, t-test); & position 6 (t(48) = 3.89, p = 0.0018, t-
 956 test). **(F)** *Slit2* expression in slices cultured with Fgf17 and BSA beads. Scale bars: 100µm.

957
 958 **Figure 10 Model.** *Hs2st* expressed in *Emx1* lineage cells catalyses 2-O HS sulphation (2-O
 959 HS) that in turn suppresses levels of Fgf17 protein, but not Fgf8 protein, by an unknown
 960 mechanism at the CSB. *Zic4* lineage astroglial precursors respond to Fgf8 and Fgf17 protein
 961 by activating FGF/ERK signalling and translocating (black arrows) to the midline. This
 962 generates appropriate positioning of *Slit2*⁺ astroglia to guide corpus callosum axons across
 963 the midline. Loss of 2-O HS from the *Emx1* lineage selectively de-suppresses Fgf17 protein
 964 levels while leaving Fgf8 protein unaffected. This causes hyperactive FGF/ERK signalling
 965 and more *Zic4* lineage astroglial precursors translocate than normal with consequent blocking
 966 of corpus callosum axon midline crossing by the ectopic midline *Slit2*⁺ astroglia. *Zic4* lineage
 967 astroglial precursor cells do not need to express 2-O HS in order to respond to FGF signalling
 968 proteins and translocate to the midline.

969

Figure 11 Ligand and carbohydrate engagement (LACE) assay for FGF:HS interactions. **(A-J, O)** FGFR1/FGF17 LACE experiments on **(A-E)** E14.5 and **(F-J)** E16.5 telencephalic coronal sections through the CSB. **(A,F)** *WT*, **(B,G)** *Hs2st*^{-/-}, **(C,H)** *Hs6st1*^{-/-} **(D,I)** *WT* sections pretreated with Heparinitase to digest HS, **(E,J)** *WT* sections with FGF17 omitted from the LACE assay. **(O)** Quantification of FGF17/FGFR1 LACE signal in *WT* (blue bar, n=9 embryos), *Hs2st*^{-/-} (green bar, n=5 embryos), and *Hs6st1*^{-/-} (purple bar, n=4 embryos), showing a significant decrease (* indicates p<0.05 on graph) in *Hs2st*^{-/-} embryos, (F(2, 15) = 8.62, p = 0.0032, ANOVA), followed by post-hoc t test: *WT* vs *Hs2st*^{-/-} (t(9) = 6.11, p = 0.014, t-test); & *WT* vs *Hs6st1*^{-/-} (t(5) = 0.63, p = 0.56, t-test) **(K-N, P)** FGFR3/FGF8 LACE experiments on E14.5 telencephalic coronal sections through the CSB. **(K)** *WT*, **(L)** *Hs2st*^{-/-}, **(M)** *WT* sections pretreated with Heparinitase to digest HS, **(N)** *WT* sections with FGF8 omitted from the LACE assay. **(P)** Quantification of FGF8/FGFR3 LACE signal in *WT* (blue bar, n=3 embryos), *Hs2st*^{-/-} (green bar, n=3 embryos) shows no significant difference (t(3) = 0.29, p = 0.76, t-test). Numbers of embryos of each genotype analysed indicated under bars. **(Q)** Summary diagram. FGFR1/FGF17/HS complex formation is equally supported by *WT* and *Hs6st1*^{-/-} HS but less so by *Hs2st*^{-/-} HS while FGFR3/FGF8/HS complex formation is equally supported by *WT* and *Hs2st*^{-/-} HS showing that FGF17:HS physical molecular interaction is selectively dependent on 2-O HS sulphation. Higher magnification showing the CSB region boxed in A-N are shown in A'-N' (note the DAPI channel is not shown in the higher magnification images to improve visualisation of the LACE signal). Scale bars 200µm.

References

- Allen, B.L., Filla, M.S., Rapraeger, A.C., 2001. Role of heparan sulfate as a tissue-specific regulator of FGF-4 and FGF receptor recognition. *J Cell Biol* 155, 845-858.
- Allen, B.L., Rapraeger, A.C., 2003. Spatial and temporal expression of heparan sulfate in mouse development regulates FGF and FGF receptor assembly. *J Cell Biol* 163, 637-648.
- Bagri, A., Marin, O., Plump, A.S., Mak, J., Pleasure, S.J., Rubenstein, J.L., Tessier-Lavigne, M., 2002. Slit proteins prevent midline crossing and determine the dorsoventral position of major axonal pathways in the mammalian forebrain. *Neuron* 33, 233-248.
- Balasubramanian, R., Zhang, X., 2016. Mechanisms of FGF gradient formation during embryogenesis. *Semin Cell Dev Biol* 53, 94-100.

- 1002 Belenkaya, T.Y., Han, C., Yan, D., Opoka, R.J., Khodoun, M., Liu, H., Lin, X., 2004.
 1003 *Drosophila* Dpp morphogen movement is independent of dynamin-mediated endocytosis but
 1004 regulated by the glypican members of heparan sulfate proteoglycans. *Cell* 119, 231-244.
 1005 Bullock, S.L., Fletcher, J.M., Beddington, R.S., Wilson, V.A., 1998. Renal agenesis in mice
 1006 homozygous for a gene trap mutation in the gene encoding heparan sulfate 2-sulfotransferase.
 1007 *Genes Dev* 12, 1894-1906.
 1008 Chan, W.K., Howe, K., Clegg, J.M., Guimond, S.E., Price, D.J., Turnbull, J.E., Pratt, T.,
 1009 2015. 2-O Heparan Sulfate Sulfation by Hs2st Is Required for Erk/Mapk Signalling
 1010 Activation at the Mid-Gestational Mouse Telencephalic Midline. *PLoS One* 10, e0130147.
 1011 Chan, W.K., Price, D.J., Pratt, T., 2017. FGF8 morphogen gradients are differentially
 1012 regulated by heparan sulphotransferases Hs2st and Hs6st1 in the developing brain. *Biol Open*
 1013 6, 1933-1942.
 1014 Cholfin, J.A., Rubenstein, J.L., 2007. Patterning of frontal cortex subdivisions by Fgf17. *Proc*
 1015 *Natl Acad Sci U S A* 104, 7652-7657.
 1016 Cholfin, J.A., Rubenstein, J.L., 2008. Frontal cortex subdivision patterning is coordinately
 1017 regulated by Fgf8, Fgf17, and Emx2. *J Comp Neurol* 509, 144-155.
 1018 Christian, J.L., 2012. Morphogen gradients in development: from form to function. *Wiley*
 1019 *Interdiscip Rev Dev Biol* 1, 3-15.
 1020 Clegg, J.M., Conway, C.D., Howe, K.M., Price, D.J., Mason, J.O., Turnbull, J.E., Basson,
 1021 M.A., Pratt, T., 2014. Heparan sulfotransferases hs6st1 and hs2st keep erk in check for mouse
 1022 corpus callosum development. *J Neurosci* 34, 2389-2401.
 1023 Conway, C.D., Howe, K.M., Nettleton, N.K., Price, D.J., Mason, J.O., Pratt, T., 2011.
 1024 Heparan sulfate sugar modifications mediate the functions of slits and other factors needed
 1025 for mouse forebrain commissure development. *J Neurosci* 31, 1955-1970.
 1026 Donahoo, A.L., Richards, L.J., 2009. Understanding the mechanisms of callosal development
 1027 through the use of transgenic mouse models. *Semin Pediatr Neurol* 16, 127-142.
 1028 Erskine, L., Williams, S.E., Brose, K., Kidd, T., Rachel, R.A., Goodman, C.S., Tessier-
 1029 Lavigne, M., Mason, C.A., 2000. Retinal ganglion cell axon guidance in the mouse optic
 1030 chiasm: expression and function of robos and slits. *J Neurosci* 20, 4975-4982.
 1031 Gobius, I., Morcom, L., Suarez, R., Bunt, J., Bukshpun, P., Reardon, W., Dobyns, W.B.,
 1032 Rubenstein, J.L., Barkovich, A.J., Sherr, E.H., Richards, L.J., 2016. Astroglial-Mediated
 1033 Remodeling of the Interhemispheric Midline Is Required for the Formation of the Corpus
 1034 Callosum. *Cell Rep* 17, 735-747.

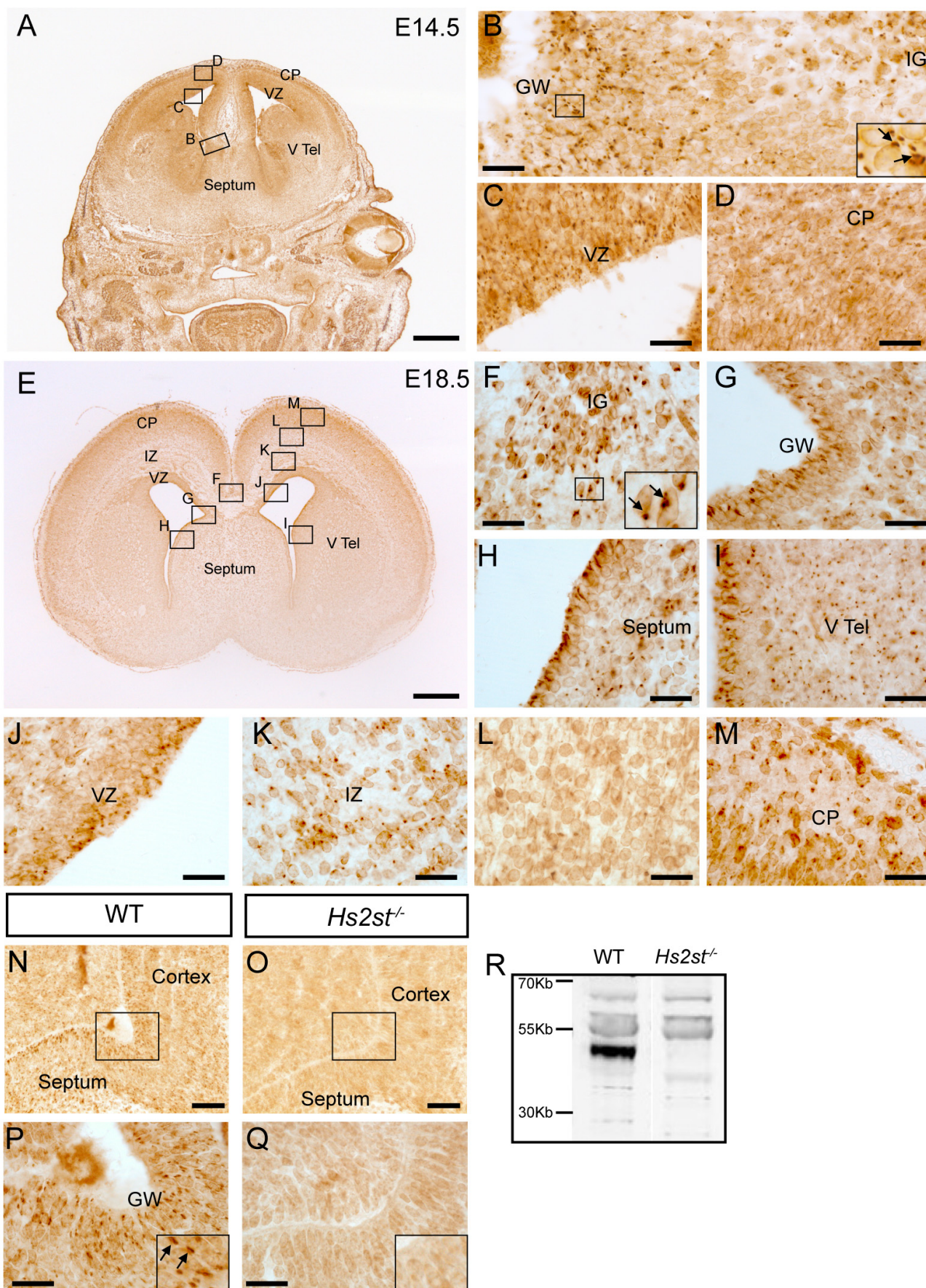
- Guillemot, F., Zimmer, C., 2011. From cradle to grave: the multiple roles of fibroblast growth factors in neural development. *Neuron* 71, 574-588.
- Hoch, R.V., Clarke, J.A., Rubenstein, J.L., 2015. Fgf signaling controls the telencephalic distribution of Fgf-expressing progenitors generated in the rostral patterning center. *Neural Dev* 10, 8.
- Inatani, M., Irie, F., Plump, A.S., Tessier-Lavigne, M., Yamaguchi, Y., 2003. Mammalian brain morphogenesis and midline axon guidance require heparan sulfate. *Science* 302, 1044-1046.
- Kessaris, N., Fogarty, M., Iannarelli, P., Grist, M., Wegner, M., Richardson, W.D., 2006. Competing waves of oligodendrocytes in the forebrain and postnatal elimination of an embryonic lineage. *Nat Neurosci* 9, 173-179.
- Kinnunen, T., Huang, Z., Townsend, J., Gatdula, M.M., Brown, J.R., Esko, J.D., Turnbull, J.E., 2005. Heparan 2-O-sulfotransferase, hst-2, is essential for normal cell migration in *Caenorhabditis elegans*. *Proc Natl Acad Sci U S A* 102, 1507-1512.
- Kreuger, J., Spillmann, D., Li, J.P., Lindahl, U., 2006. Interactions between heparan sulfate and proteins: the concept of specificity. *J Cell Biol* 174, 323-327.
- Li, J.P., Kusche-Gullberg, M., 2016. Heparan Sulfate: Biosynthesis, Structure, and Function. *Int Rev Cell Mol Biol* 325, 215-273.
- Loo, B.M., Kreuger, J., Jalkanen, M., Lindahl, U., Salmivirta, M., 2001. Binding of heparin/heparan sulfate to fibroblast growth factor receptor 4. *J Biol Chem* 276, 16868-16876.
- Loo, B.M., Salmivirta, M., 2002. Heparin/Heparan sulfate domains in binding and signaling of fibroblast growth factor 8b. *J Biol Chem* 277, 32616-32623.
- Makarenkova, H.P., Hoffman, M.P., Beenken, A., Eliseenkova, A.V., Meech, R., Tsau, C., Patel, V.N., Lang, R.A., Mohammadi, M., 2009. Differential interactions of FGFs with heparan sulfate control gradient formation and branching morphogenesis. *Sci Signal* 2, ra55.
- Matsumoto, Y., Irie, F., Inatani, M., Tessier-Lavigne, M., Yamaguchi, Y., 2007. Netrin-1/DCC signaling in commissural axon guidance requires cell-autonomous expression of heparan sulfate. *J Neurosci* 27, 4342-4350.
- Moldrich, R.X., Gobius, I., Pollak, T., Zhang, J., Ren, T., Brown, L., Mori, S., De Juan Romero, C., Britanova, O., Tarabykin, V., Richards, L.J., 2010. Molecular regulation of the developing commissural plate. *J Comp Neurol* 518, 3645-3661.

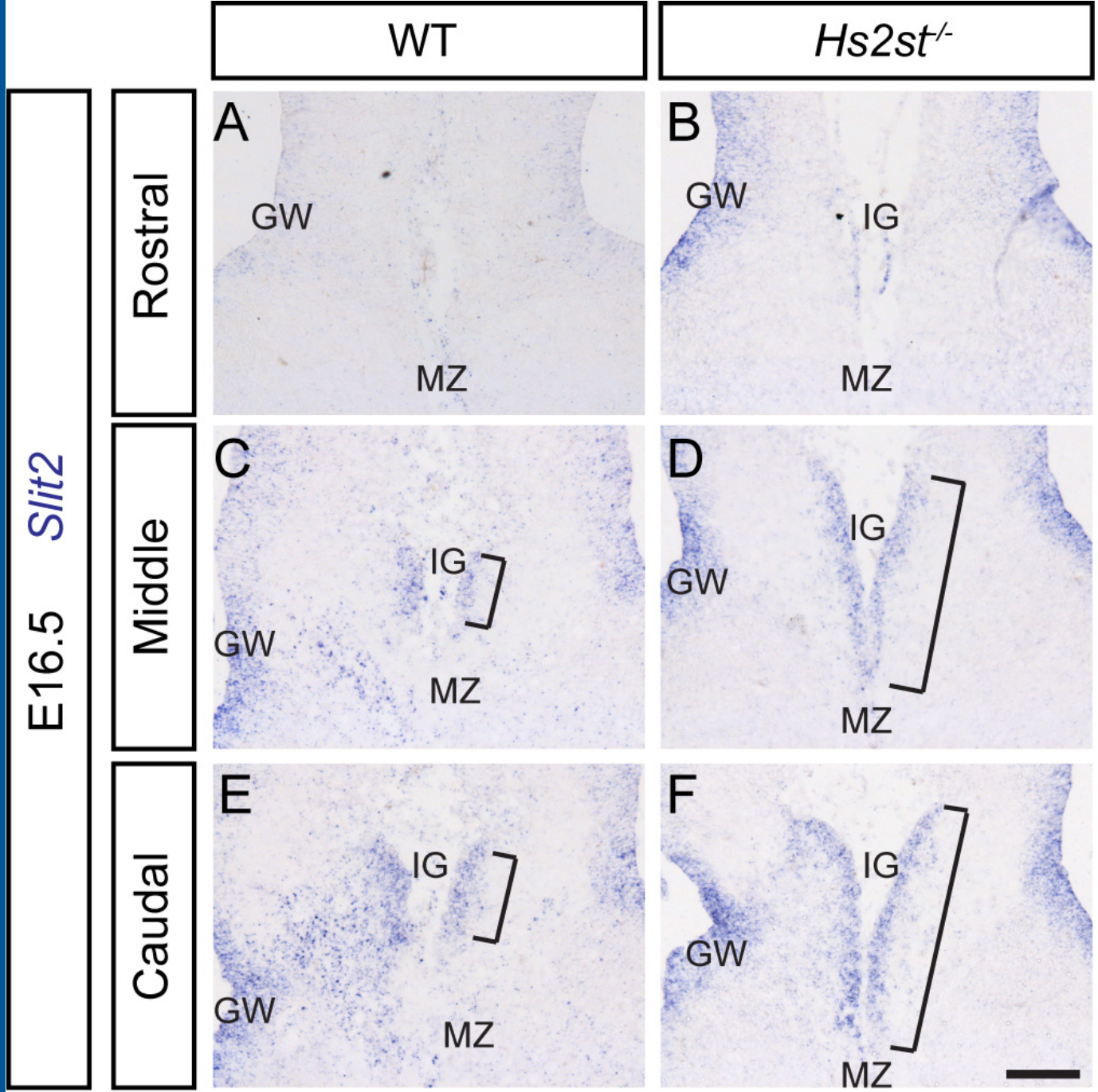
- 1067 Niquille, M., Garel, S., Mann, F., Hornung, J.P., Otsmane, B., Chevalley, S., Parras, C.,
 1068 Guillemot, F., Gaspar, P., Yanagawa, Y., Lebrand, C., 2009. Transient neuronal populations
 1069 are required to guide callosal axons: a role for semaphorin 3C. *PLoS Biol* 7, e1000230.
 1070 Ornitz, D.M., Itoh, N., 2015. The Fibroblast Growth Factor signaling pathway. Wiley
 1071 *Interdiscip Rev Dev Biol* 4, 215-266.
 1072 Piper, M., Anderson, R., Dwivedy, A., Weinl, C., van Horck, F., Leung, K.M., Cogill, E.,
 1073 Holt, C., 2006. Signaling mechanisms underlying Slit2-induced collapse of *Xenopus* retinal
 1074 growth cones. *Neuron* 49, 215-228.
 1075 Pratt, T., Conway, C.D., Tian, N.M., Price, D.J., Mason, J.O., 2006. Heparan sulphation
 1076 patterns generated by specific heparan sulfotransferase enzymes direct distinct aspects of
 1077 retinal axon guidance at the optic chiasm. *J Neurosci* 26, 6911-6923.
 1078 Pratt, T., Sharp, L., Nichols, J., Price, D.J., Mason, J.O., 2000. Embryonic stem cells and
 1079 transgenic mice ubiquitously expressing a tau-tagged green fluorescent protein. *Dev Biol*
 1080 228, 19-28.
 1081 Qu, X., Carbe, C., Tao, C., Powers, A., Lawrence, R., van Kuppevelt, T.H., Cardoso, W.V.,
 1082 Grobe, K., Esko, J.D., Zhang, X., 2011. Lacrimal gland development and Fgf10-Fgfr2b
 1083 signaling are controlled by 2-O- and 6-O-sulfated heparan sulfate. *J Biol Chem* 286, 14435-
 1084 14444.
 1085 Qu, X., Pan, Y., Carbe, C., Powers, A., Grobe, K., Zhang, X., 2012. Glycosaminoglycan-
 1086 dependent restriction of FGF diffusion is necessary for lacrimal gland development.
 1087 *Development* 139, 2730-2739.
 1088 Ramsbottom, S.A., Maguire, R.J., Fellgett, S.W., Pownall, M.E., 2014. Sulf1 influences the
 1089 Shh morphogen gradient during the dorsal ventral patterning of the neural tube in *Xenopus*
 1090 *tropicalis*. *Dev Biol* 391, 207-218.
 1091 Rubin, A.N., Alfonsi, F., Humphreys, M.P., Choi, C.K., Rocha, S.F., Kessaris, N., 2010. The
 1092 germinal zones of the basal ganglia but not the septum generate GABAergic interneurons for
 1093 the cortex. *J Neurosci* 30, 12050-12062.
 1094 Shimokawa, K., Kimura-Yoshida, C., Nagai, N., Mukai, K., Matsubara, K., Watanabe, H.,
 1095 Matsuda, Y., Mochida, K., Matsuo, I., 2011. Cell surface heparan sulfate chains regulate
 1096 local reception of FGF signaling in the mouse embryo. *Dev Cell* 21, 257-272.
 1097 Shu, T., Richards, L.J., 2001. Cortical axon guidance by the glial wedge during the
 1098 development of the corpus callosum. *J Neurosci* 21, 2749-2758.
 1099 Shu, T., Sundaresan, V., McCarthy, M.M., Richards, L.J., 2003. Slit2 guides both precrossing
 1100 and postcrossing callosal axons at the midline in vivo. *J Neurosci* 23, 8176-8184.

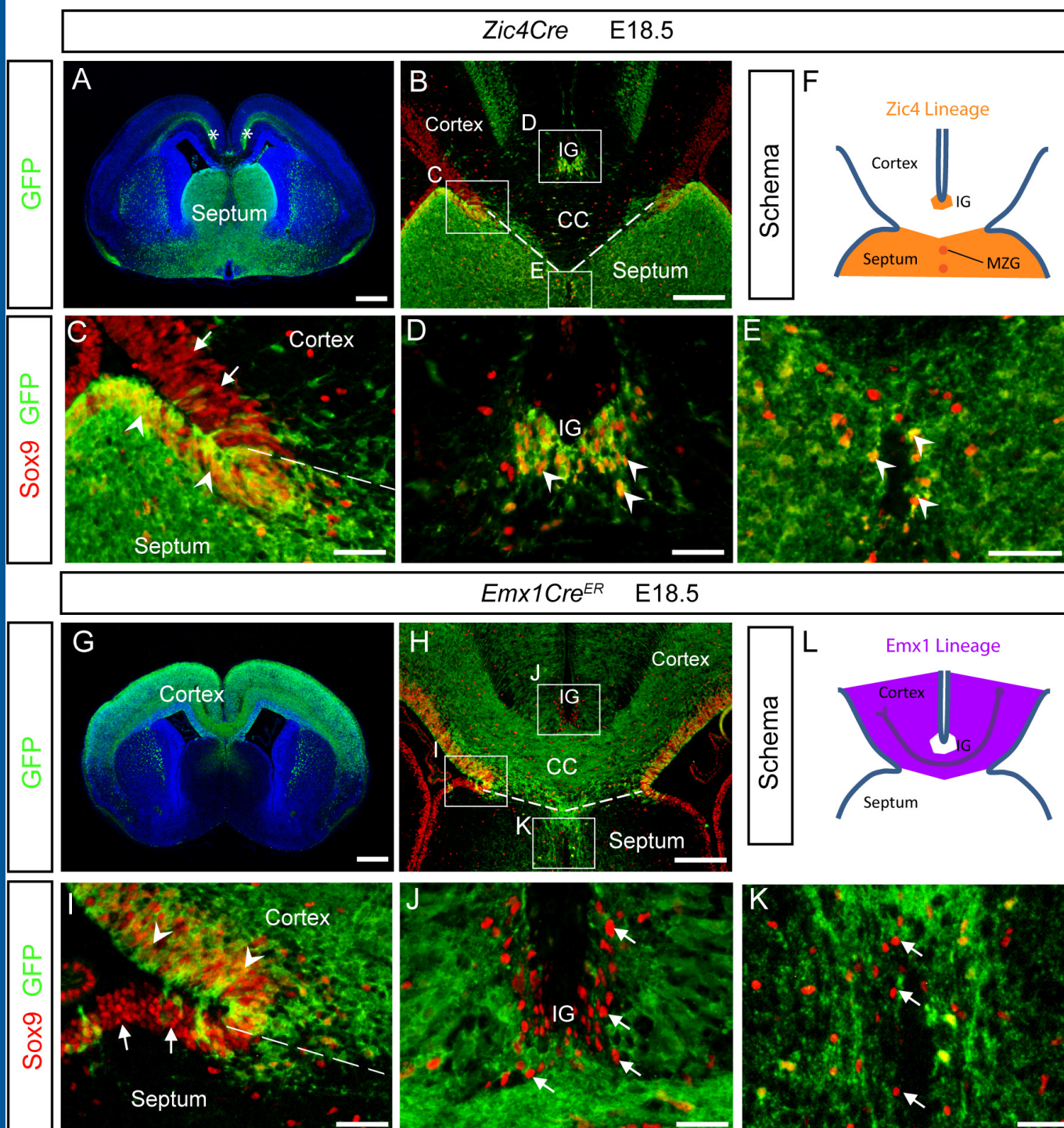
- 1101 Smith, K.M., Ohkubo, Y., Maragnoli, M.E., Rasin, M.R., Schwartz, M.L., Sestan, N.,
 1102 Vaccarino, F.M., 2006. Midline radial glia translocation and corpus callosum formation
 1103 require FGF signaling. *Nat Neurosci* 9, 787-797.
- 1104 Sousa, V.H., Miyoshi, G., Hjerling-Leffler, J., Karayannis, T., Fishell, G., 2009.
 1105 Characterization of Nkx6-2-derived neocortical interneuron lineages. *Cereb Cortex* 19 Suppl
 1106 1, i1-10.
- 1107 Stanford, K.I., Wang, L., Castagnola, J., Song, D., Bishop, J.R., Brown, J.R., Lawrence, R.,
 1108 Bai, X., Habuchi, H., Tanaka, M., Cardoso, W.V., Kimata, K., Esko, J.D., Heparan sulfate 2-
 1109 O-sulfotransferase is required for triglyceride-rich lipoprotein clearance. *J Biol Chem* 285,
 1110 286-294.
- 1111 Toyoda, R., Assimacopoulos, S., Wilcoxon, J., Taylor, A., Feldman, P., Suzuki-Hirano, A.,
 1112 Shimogori, T., Grove, E.A., 2011. FGF8 acts as a classic diffusible morphogen to pattern the
 1113 neocortex. *Development* 137, 3439-3448.
- 1114 Turnbull, J., Powell, A., Guimond, S., 2001. Heparan sulfate: decoding a dynamic
 1115 multifunctional cell regulator. *Trends Cell Biol* 11, 75-82.
- 1116 Wallace, V.A., Raff, M.C., 1999. A role for Sonic hedgehog in axon-to-astrocyte signalling
 1117 in the rodent optic nerve. *Development* 126, 2901-2909.
- 1118 Wang, Y., Kim, E., Wang, X., Novitch, B.G., Yoshikawa, K., Chang, L.S., Zhu, Y., 2012.
 1119 ERK inhibition rescues defects in fate specification of Nf1-deficient neural progenitors and
 1120 brain abnormalities. *Cell* 150, 816-830.
- 1121 Xu, J., Lawshe, A., MacArthur, C.A., Ornitz, D.M., 1999. Genomic structure, mapping,
 1122 activity and expression of fibroblast growth factor 17. *Mech Dev* 83, 165-178.
- 1123 Yan, D., Lin, X., 2009. Shaping morphogen gradients by proteoglycans. *Cold Spring Harb*
 1124 *Perspect Biol* 1, a002493.
- 1125 Yu, S.R., Burkhardt, M., Nowak, M., Ries, J., Petrasek, Z., Scholpp, S., Schwille, P., Brand,
 1126 M., 2009. Fgf8 morphogen gradient forms by a source-sink mechanism with freely diffusing
 1127 molecules. *Nature* 461, 533-536.
- 1128 Zhang, H., Newman, D.R., Sannes, P.L., 2012a. HSULF-1 inhibits ERK and AKT signaling
 1129 and decreases cell viability in vitro in human lung epithelial cells. *Respir Res* 13, 69.
- 1130 Zhang, X., Bao, L., Yang, L., Wu, Q., Li, S., 2012b. Roles of intracellular fibroblast growth
 1131 factors in neural development and functions. *Sci China Life Sci* 55, 1038-1044.

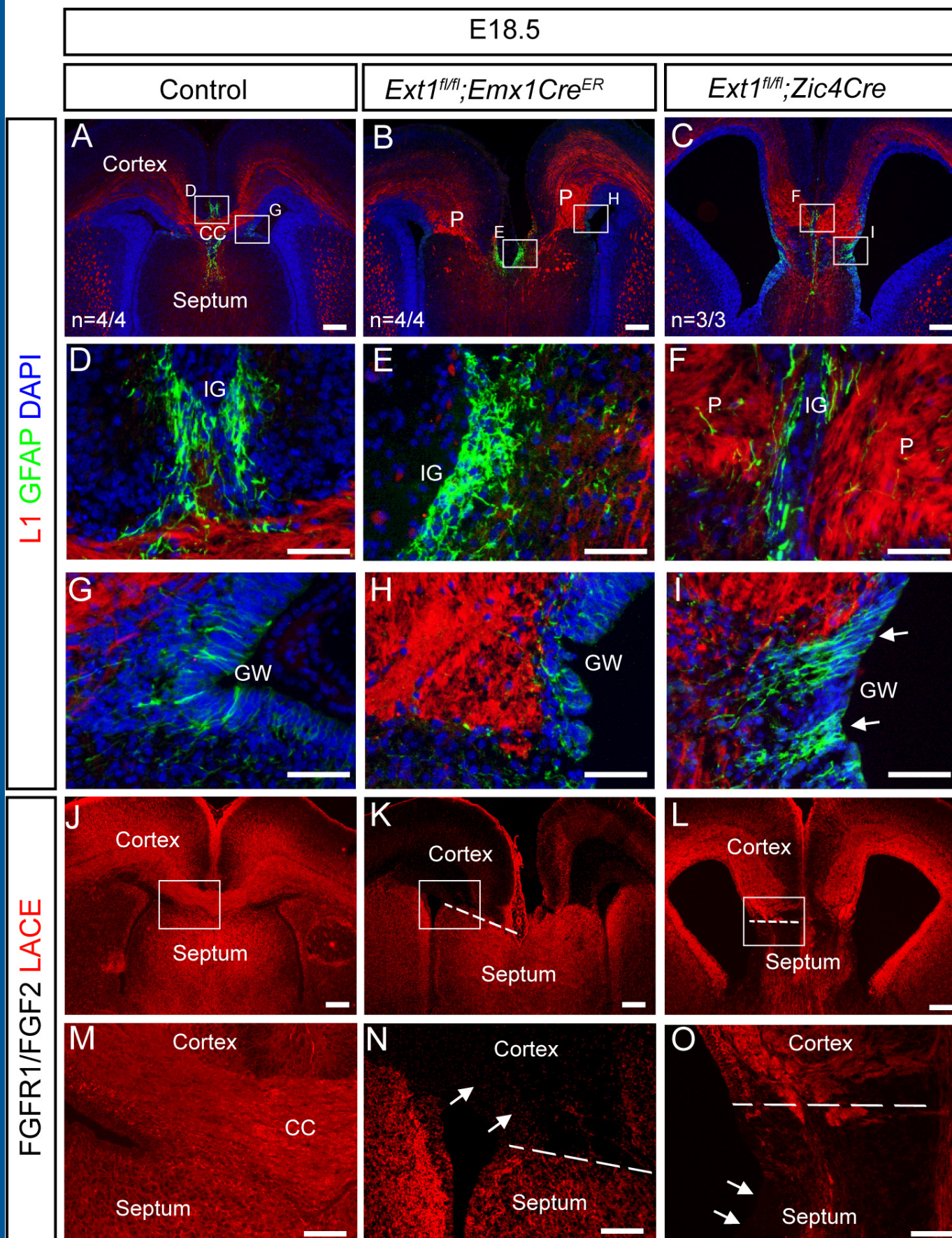
1132

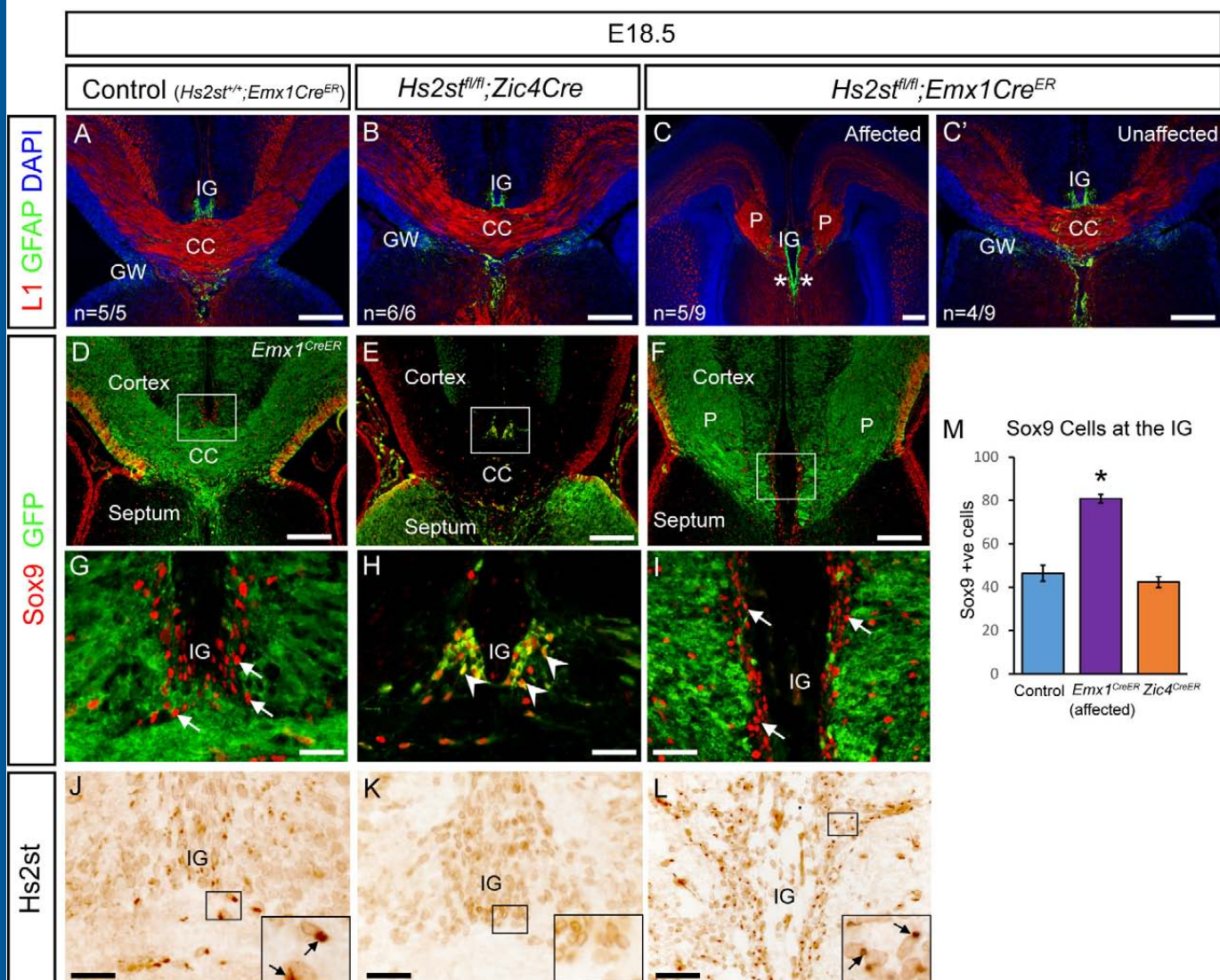
Hs2st

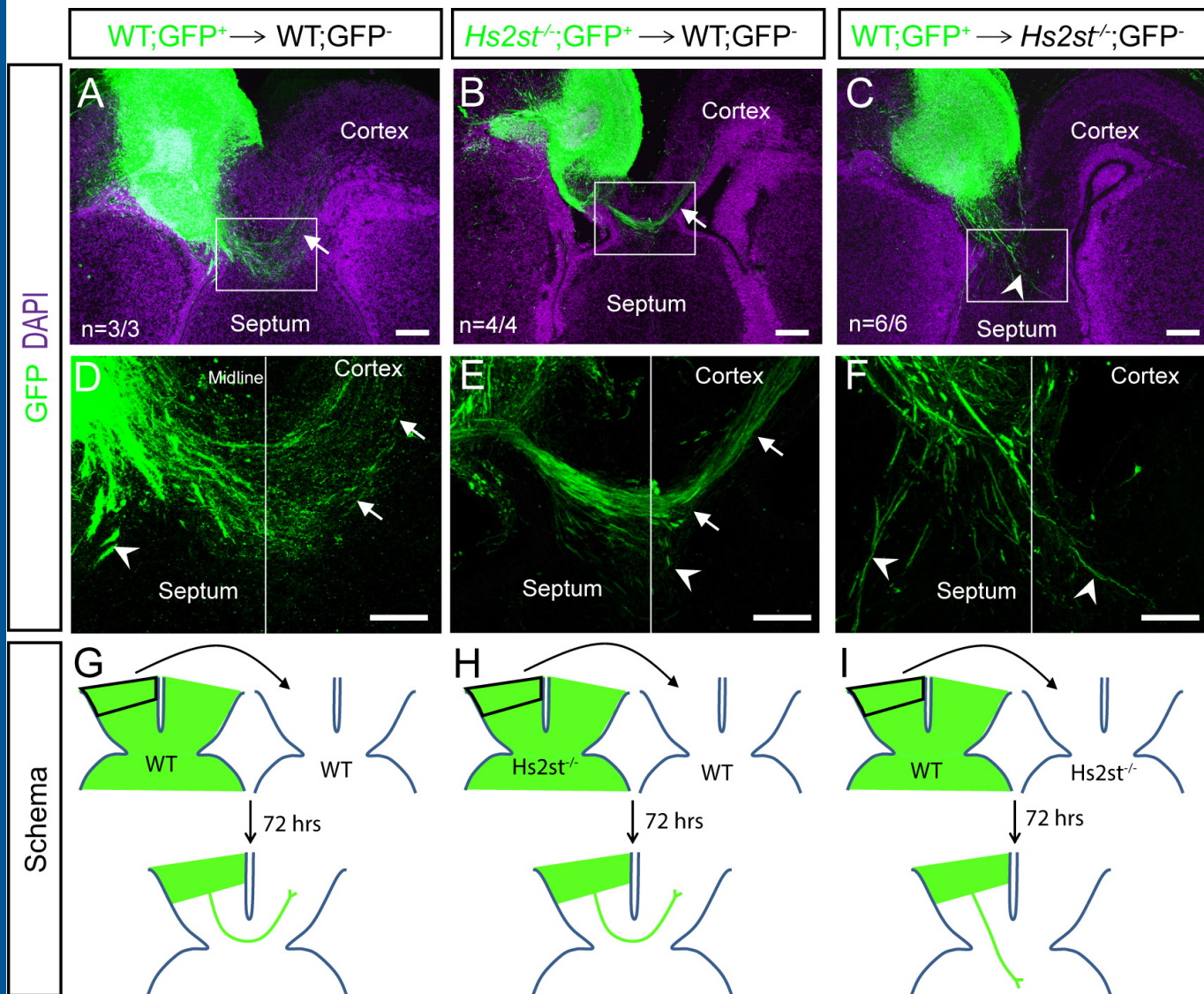


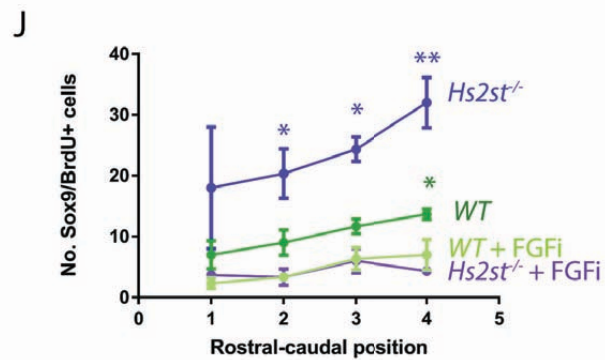
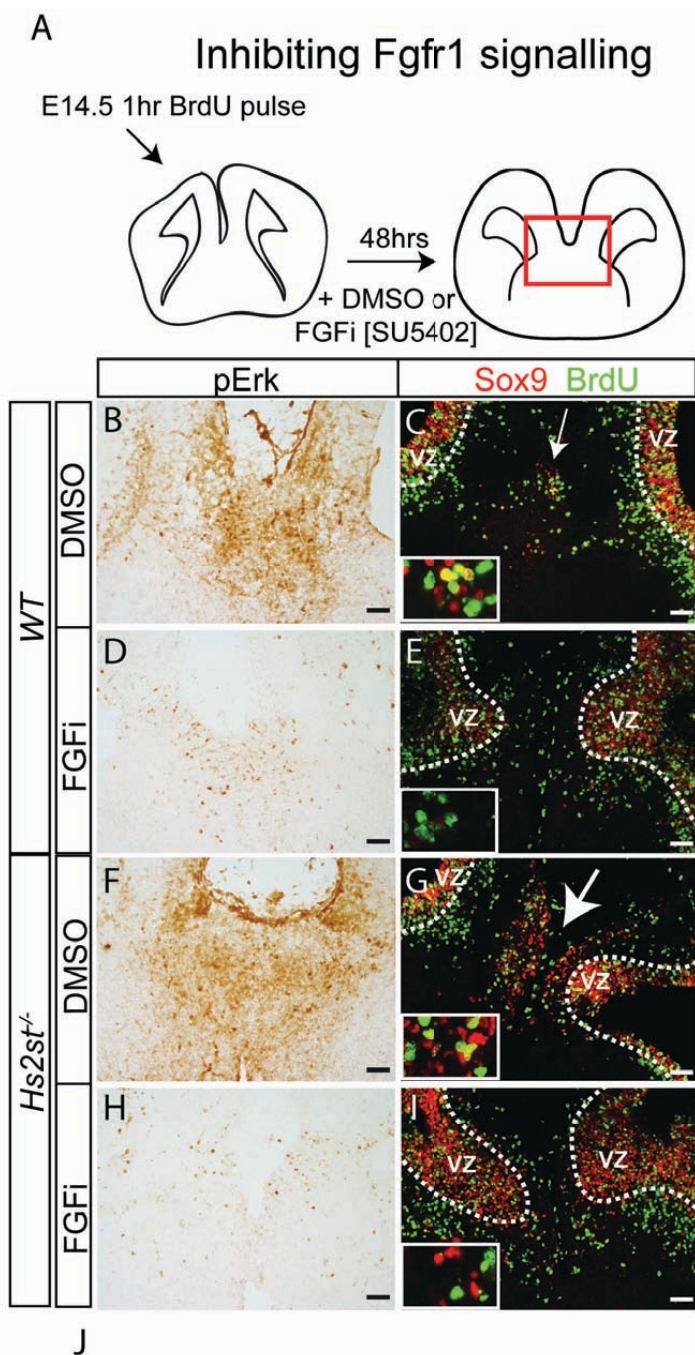


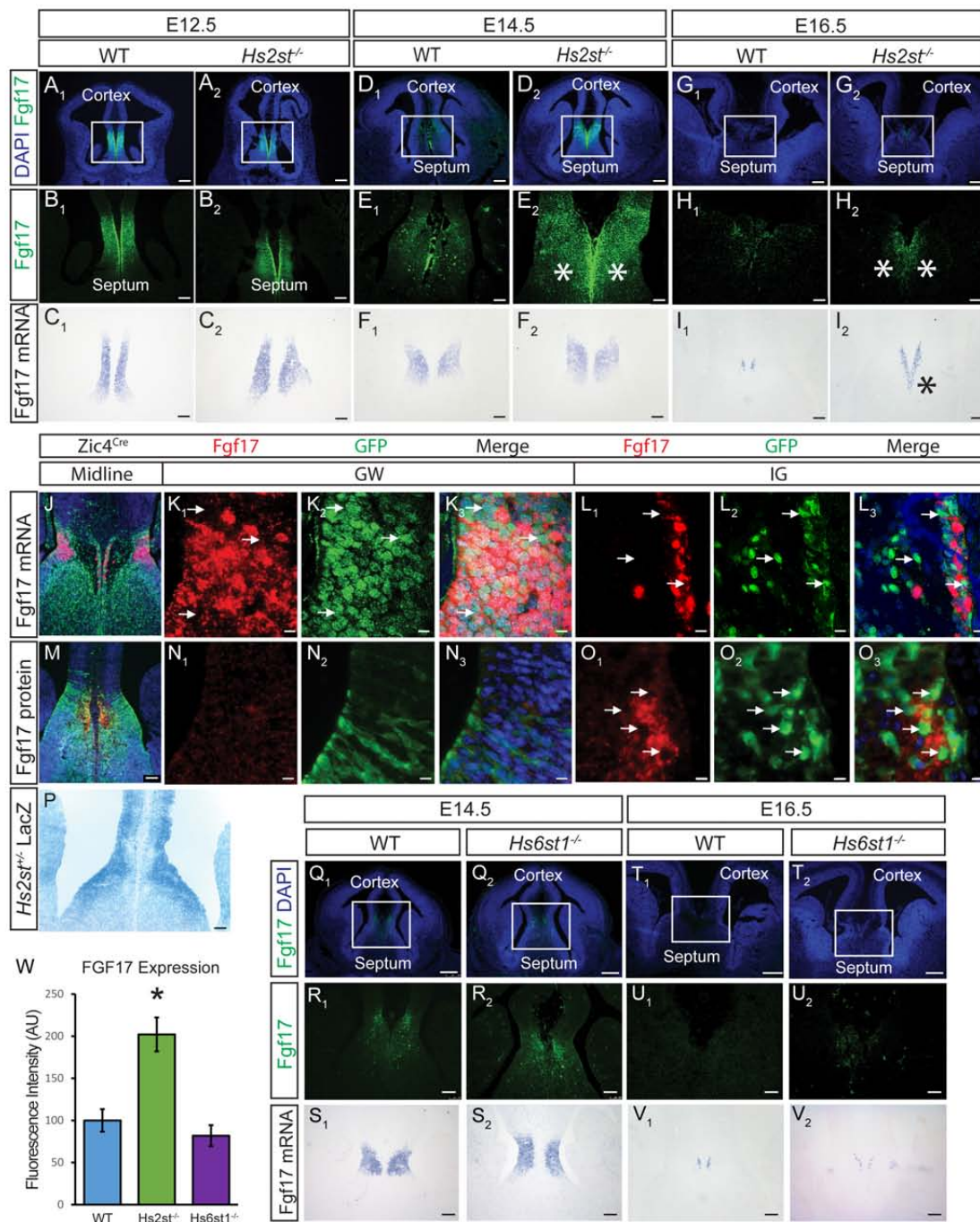












A

Ectopic expression of Fgf17

E14.5 1hr BrdU pulse

